PETROGRAPIC AND LITHO-GEOCHEMICAL CHARACTERIZATION OF THE VMS DEPOSIT AT EL ROBLE MINE, COLOMBIAN WESTERN CORDILLERA

Elaborated by:

Jose Manuel Murillo Bedoya

Bachelor thesis presented as required to obtain the title of Geologist

Director:

Maria Isabel Marín Cerón

Advisors:

Balmer Echeverri Franco
Sebastián Echeverry Castañeda

ATICO Mining
Exploration Area

EAFIT University
School of Sciences
Earth Science Department
Medellín, Colombia
2020

CONTENTS

PREFACE

This study is presented as a manuscript to be submitted to the Economic Geology journal. Additional material attached includes, petrography description, other geochemistry graphs and digitalized thin sections. The geodatabase is restricted by the company policies so it will not be included to this work. I gratefully acknowledge the financial and logistics support of Minera El Roble and Atico Mining Corporation in the development of this research, especially the geologists and field assistants exploration department who accompanied the fieldwork: Ever Gonzalez, Sady Barreto, Sebastián Echeverry, John Camilo Zapata and our assistants Mauricio, Jorge and Pablo. Of course, future challenges are waiting to be solved and I hope Minera El Roble and specially Balmer Echeverri will continue supporting science and learning in Colombia. Finally, special thanks to my thesis director Maria Isabel Marin for being so supportive.

Hypothesis

- El Roble is a Siliciclastic – Mafic VMS deposit, related to successions of mafic volcanic rocks and shallow marine sedimentary rocks.

Objectives

General Objective

To understand the litho-geochemical characterization of El Roble mine to determine the type of VMS deposit.

Specific Objectives

- To build a geological database of El Roble mine from 90.000 meters of drill-cores to select the samples for litho-geochemical analysis.
- To determine petrographic characteristics of selected samples.
- To determine geochemical characteristics of selected samples.
- To apply chemical vectors as an exploration tool.
- To discuss the above-mentioned dataset for the understanding of the VMS type and its implications on exploration targets.

PETROGRAPIC AND LITHO-GEOCHEMICAL CHARACTERIZATION OF THE VMS DEPOSIT AT EL ROBLE MINE, COLOMBIAN WESTERN CORDILLERA

Murillo-Bedoya J.M. Marín-Cerón, M.I. Echeverri-Franco B. Castañeda-Echeverry S.

ABSTRACT

El Roble Mine (Cu-Au) siliciclastic-mafic volcanogenic massive sulfide (VMS) deposit, is located at El Carmen de Atrato, Chocó, Colombian Western Cordillera. This 4-million-ton VMS occurs replacing black chert rocks between Upper Cretaceous volcanic Barroso Formation and Upper Cretaceous Urrao member of Penderisco Formation. Major, trace and REE elements, indicate that there are at least two different mantle sources (E-MORB and N-MORB) from the volcanic Barroso Formation(?). Then the close relation between black chert unit and E-MORB related basalts may have leaded the VMS mineralization. The 2D geochemical vector modelling from drill-cores around "Zeus" ore body shows positive correlated anomalies for the AI (Alteration Index), CCPI (Chlorite Carbonate Pyrite Index), Tl and MgO with the presence of hyaloclastites, becoming important exploration vectors for the VMS at the North Volcanic Zone of the Andean Cordillera. Nevertheless, the Na_2O negative anomaly close to the ore body, is not conclusive in such type of VMS due to overprinted hydrothermal alteration closely related to the Cenozoic arc environment.

1. INTRODUCTION

Volcanogenic Massive Sulfides (VMS) are formed in extensional sea floor environments (**Figure 1**) from hydrothermal fluids associated with contemporaneous volcanism in strata-bound concentrations with lensoidal or sheet-like form (Shanks and Thurston, 2012). This kind of deposits are still forming in modern oceanic settings, however, some of the most productive are emplaced in the continents (**Figure 2**) (Franklin et al., 2005), and they are the important source of metals (e.g. copper, zinc, lead, silver and gold, among others) (Shanks and Thurston, 2012).

El Roble mine is a (4M ton) VMS deposit located in the Western Cordillera of Colombia, with an association of chalcopyrite, pyrite, pyrrhotite, sphalerite and other sulfide minerals that are part of the Volcanic Massive Sulfide deposit (Atico Mining, 2020). The mine is located 3 km away from El Carmen de Atrato (**¡Error! No se encuentra el origen de la referencia.Figure**

3) town, around 1800 meters above the sea level and it is around 140 km south west of Medellin City, Colombia (Atico Mining, 2020). The regional geology (**Figure 4**) corresponds to interbedded claystones, mudstones, sandstones, cherts, conglomerates, tuffs and some turbidites from the Urrao member of the Penderisco Formation (Upper Cretaceous). Moreover, spilitized basaltic lava flows, tuffs and basalts from Cretaceous Barroso Formation have been reported (Ingeominas et al., 1986).

Until now, the available dataset from El Roble deposit, may indicate a Siliciclastic-Mafic related VMS, associated with subequal portions of mafic and siliciclastic rocks (**Figure 5**a**¡Error! No se encuentra el origen de la referencia.**), where the ultramafic intrusive rocks are common and felsic rocks could be found with fewer quantity (Piercey, 2009). Such association is usually related to an accreted and juvenile arc environment and in oceanic mature back-arc settings (Franklin et al., 2005). In this type of VMS, the sulfide metals are mainly replacing host sediments from the sedimentary pile as shown in (**Figure 5**a**¡Error! No se encuentra el origen de la referencia.**) (Shanks and Thurston, 2012). Nevertheless, such hypothesis must be confirmed. Moreover, during the mine operation (ca. 30 years) several geologists have been classifying the related rocks using empiric nomenclature that do not have a clear geological meaning, thus a detailed petrographic and geochemical study is needed to setup new exploration targets.

Therefore, this research uses geodatabase consolidation, conventional petrographic analyses (19 thin sections) together with whole rock geochemical characterization (major, minor, trace and REE elements), to determine the volcanic and sedimentary textures, replacement minerals and their plausible tectonic setting in a VMS deposit. Finally, geochemical vectors (such as major, minor and REE elements such as Na, Mg, Tl, and alteration indexes), were used to highlight future exploration targets.

2.TECTONIC AND GEOLOGICAL SETTING

Tectonic setting for northwestern Colombia includes accreted rocks of the eastern Choco Arc preserved as the Cañas Gordas terrane (Cediel and Shaw, 2019). A series of events starting with the post Maastrichtian accretion of the Cañas Gordas terrane to the continental margin along the Garrapatas – Dabeiba Suture, followed by Eocene emplacement of El Paso-Baudó terrane represented with the San Juan – San Sebastian Suture, then 8 – 4Ma uplift of the Baudó range and the last one was at 4Ma the formation of the Colombian trench (Redwood, 2019). Aptian Albian Barroso formation (Rodríguez García and Arango Mejía, 2013) and the Campanian - Maastrichtian Urrao Member are related to the interaction between Caribbean and South American plates resulting in an oceanic arc - continent collision resulting in foreland and hinterland basins, clastic rocks were accumulated in short depositional systems in deep marine settings (Pardo-Trujillo et al., 2020). Volcano-sedimentary

The geological setting includes volcano-sedimentary rocks from the Barroso Formation and the sedimentary Urrao member (Penderisco Formation), these sequences are folded, and structural reconstruction is not well understood at El Roble mine. La Mansa fault is controlling the general structures of the study area, with a NW-SE direction, verging to the east, but locally planes are found oppositely verging; authors propose this fault to be normal (Ingeominas et al., 1986; Espada, 2012). The deposition of sedimentary Barroso seems to be associated with normal faults that then were inverted during late phases of the Andean orogeny (Ingeominas et al., 1986; Espada, 2012). A detailed explanation of each geological unit is presented here after.

2.1 Barroso Formation

According to Alvarez (1971) the Barroso Formation is formed by volcanic rocks varying in composition and texture, from aphanitic to porphyritic lava flows. The lithology in order of

abundance corresponds to diabases, basalts, porphyritic basalts, agglomerates, breccias and spilites. This work will focus on El Carmen de Atrato (Chocó) area, where the general lithology is related to diabase - dark cherts interbedding, with an intense hydrothermal mineralization along El Roble mine (Álvarez and González, 1978) and (Atico Mining, 2020).

The Barroso Formation (Turonian – Aptian, 88 – 115 Ma Ar-Ar in whole rock; Rodríguez García & Arango Mejía, 2013), contains abundant fossils near the towns of Ciudad Bolivar and El Carmen de Atrato; they have been reported as Turonian and Maastrichtian – Campanian (Etayo et al., 1980). Up to now, the provenance analysis indicates a wide range of ages, suggesting multiple sedimentary cycles represented on Barroso sedimentary sequence (Rodríguez García and Arango Mejía, 2013). The Barroso Formation is also intruded by several igneous bodies such as the Mandé Batholith (U–Pb zircon age of 43–42 Ma; Ingeominas et al., 1986; Villagómez et al., 2011).

2.2 Penderisco Formation

The Late Cretaceous Penderisco Formation, described by (Ingeominas et al., 1986; Pardo-Trujillo et al., 2020) includes deep – marine turbidites and hemi – pelagic sedimentary rocks, it is divided into two members: (1) The Nutibara Member, outcropping to the west of the study area, related to cherts, mudstones, micritic limestones and shales. (2) The Urrao member is found in the study area as interbedded claystones, mudstones, sandstones, cherts, and conglomerates, with a wide variation on their physical characteristics. Regionally it is disposed in a wide anticline, with at least two phases of folding (Espada, 2012). This succession is related to submarine fans (**Figure 6**) accumulated in levees channels and lobes in short depositional systems, with coetaneous volcanism, where the continental paleo-margin was the main source of the Urrao member sediments (Pardo-Trujillo et al., 2020). Detrital zircon and

macro and microfossil information indicates a maximum depositional age of 79-73 Ma (Campanian – Maastrichtian) (Pardo-Trujillo et al., 2020).

3. METHODOLOGY

Sixteen samples for litho-geochemistry and 19 for petrography collected from drill core, including those available at El Roble mine drill core cellar following an E-W transect (at an altitude of 1760 m.a.s.l). Structural, field and core drilling data for the above-mentioned section was taken from previous exploration campaigns and other studies (Espada, 2012).

3.1 Geodatabase compilation of drill cores

The compiled geodatabase from El Roble mine, is composed by more than 90000 meters of drill cores, for visual displaying it is used Datamine-Discover 2017®. The sampling was done creating a plane projection (1760 m.a.s.l.), using a solid buffer of 30 meters, trying to cover all kinds of lithology near to the mineralized body called "Zeus" (**Figure 7**). Geodatabase was also complemented with previous cartography, stratigraphical and geochemical published data (Ingeominas et al., 1986; Rodríguez García and Arango Mejía, 2013; Pardo-Trujillo et al., 2020). Finally, drillhole lithology and structures interpretation helped us to build the generalized 2D stratigraphical sections (**Figure 8** and **¡Error! No se encuentra el origen de la referencia.Figure 9**).

3.2 Petrographic characterization

Nineteen thin sections were prepared and analyzed at Gmas lab.

Digitalization of the thin sections under the microscope was done in parallel and crossed Nicholls using OneGeo®, to get a 450mpx ultra high-resolution image (every 5 degrees that

aloud to have a virtual microscope). A total of 7 samples were interpreted and 5 samples were chosen to perform XRD analysis at Gmas lab, using a diffractometer Bruker D4 Endeavor with a K alpha λ =1.5406, nickel filter 40KV 30mA, samples were reduced to a powder of less than 63 microns. Finally, XRD results were compared with a data base using the software EVA® at Gmas lab (Gmas, 2020).

3.3 Geochemical Characterization

Whole-rock geochemistry samples were prepared at ALS-Colombia and analyzed at ALS Vancouver Canada. Major elements were analyzed using fusion X-ray fluorescence. LOI for XRF calculation was done using WST-SEQ. Trace and REE elements were analyzed by four acid digestion followed by ICP-MS (inductively coupled plasma-mass spectrometry) (ALS, 2020a). Whole rock by fusion high total was obtained due to sulphides being calculated twice (in the LOI value and retained in the fusion adding to the XRF total). The sulfur-free total calculation is the total minus SO_3. In general, the SF-Total was less than or equal to 100% (ALS, 2020b; ALS, 2020c; ALS, 2020a).

Precision and accuracy of the analyses were determined using a Standard Oreas® 600 sample and an SGS® certified coarse quartz blank sample. Geochemical data was plotted using IoGas® and Excel. Finally, a basic Topo to Raster interpolation using ArcGis pro® together with elevation profiles were used to identify chemical variation across the transect.

4.RESULTS

4.1 Geodatabase compilation of drill cores

Drill cores around El Roble area were chosen as shown in **Figure 10**, using a 3D interpretation geology, complemented by the 2D mineralized bodies model done in Autocad® using Datamine – Discover 3D®.

It is possible to identify in **Figure 7** the normal faults that control sedimentary processes related to possible horsts and grabens typical in rift associated settings. Mineralized bodies are elongated S-N direction same as black chert unit replacing the original lithology. A peperitic contact (mixture between non-consolidated sediments with erupting lavas under ocean water, White et al., 2000)) between black chert and E-MORB hyaloclastites followed by stockworks in the N-MORB basalts. E-MORB diabase appear in the furthest area.

4.2 Petrographic characterization

As mentioned before 19 thin sections were used to classify the lithologies at the study area such as: volcanic rocks (basalts and dikes) and sedimentary rocks (black chert and gray claystone). A generalized stratigraphic column (**Figure 5**b) for the study area was redefined using texture and the tectonic setting criteria for the "volcanic basement" (e.g. The Barroso Formation and "porphyry andesite dike"). The sedimentary rocks are the same as those proposed. The section A (**Figure 9**) show the interpreted associated lithologies affected by intense folding (vertical dipping) arranged in a series of narrow anticline and synclines (Espada, 2012).

4.2.1 Volcanic rocks

Volcanic rocks will be described starting from the closest rocks to the ore body "Zeus" to the furthest rocks at approx. 180m away.

Hyaloclastites are formed by non-explosive volcanic eruptions in which water is involved consisting on glassy fragmental debris usually with basaltic composition (Batiza and White, 2007; Gill, 2010). The previous description matches with the rocks (e.g ERMP-001 - **Figure 11**) seen at 20m from the ore body, these are composed of a glassy matrix with chlorite, secondary biotite and some crystals of plagioclase, hornblende and few opaque minerals such as pyrite, nimite and thyrodite (determined by XRD). Deformation was also identified by the presence of undulatory extinction on quartz and lobular contacts. Hyaloclastites are altered by ocean floor metasomatism.

Another group of micro-porphyry volcanic rock extremely hydrothermally altered to clay with fibrous to acicular habit, chlorite, calcite and opaque minerals, are found at 80m from the ore body, even with this alteration, some relicts of the original texture could be recognized such as elongated, and well-developed crystals embedded in a fine matrix. Minerals such as plagioclase interdigitated with clinopyroxene could be recognized within the bands forming sub-ophitic texture. Two main phases are recognized, among the stockwork area, altered host basalts and dikes forming the reticular setting (ERMP-004, **Figure 12**).

As explained previously, the stockwork (16-17Ma zircon U-Pb analyses from De Brito et al., (2010)), is formed by range of lithologies between trachy-basalts to trachy-dacites with porphyritic texture, with subhedral to euhedral plagioclase, amphibole, plus +/- quartz, and k-feldspar phenocrysts. Groundmass is composed of micro-phenocrystals of plagioclase amphiboles and +/- quartz. Is noticeable a strong blue pleochroism in amphiboles confirming

high sodium content (**Figure 13**) (Nesse, 1986). In general, those samples are fractured and filled by millimetric carbonate veins. A weak argillic alteration is found (sericite, chlorite).

At 160 m there is an idiomorphic igneous rock composed of small anhedral calcic plagioclase in a fine augite matrix. Crystals are partially altered to clinochlor hornblende and thyrodite (determined by XRD). There are also some olivine crystals. The rock is classified as a Diabase (ERMP – 014 **Figure 14**)

4.2.2 Sedimentary rocks

Dark chert rocks appear as host of VMS mineralization and it is overlaying basalts in the sequence. They are formed principally by micro to crypto crystalline silica and the presence of organic matter is responsible of the dark color. There are silicified floating bioclasts embedded in a microcrystalline matrix parallel to stratification. Variations in the fabric are showing recrystallization and an increment in organic matter as interlamination. Lenticular areas in the rock could be ichnofossils. Numerous veins in a reticular setting are also found, moreover styloliths with organic matter are associated with those veins. Porosity is poor and it is represented by thin fractures with poor lateral continuity. (ERMP-009 **Figure 15**).

Being part of the same unit there are wake-stone and cherts. Those rocks are distributed in bands of chert and limestone, with gradational contacts. Cryptocrystalline quartz and calcite are found within them. Globose foraminifera fossils are disseminated, floating in micrite, and sometimes agglomerated within parallel bands to the stratification. styloliths are frequently found with organic matter trapped inside. Veins occluded with calcite and dolomite in less proportion are perpendicularly cutting the stratification. Porosity is poor and corresponds to fractures. (**Figure 16**). According those characteristics they can be classified as fossiliferous micritic limestone (Folk, 1974).

Claystone are found as laminated clay matrix with homogeneous extinction, other components such as agglutinant foraminifera, organic matter, microcrystalline quartz, and veins filled with siderite are found (ERMP – 002 **Figure 17**). Fractured stylolithic surfaces are filled with organic matter and micro faults.

4.3 Geochemistry

Geochemical data is presented in **Table 1**, **Table 2** and **Table 3**.

4.3.1 Major and minor elements

TAS classification diagram from Le Bas and Streckeisen, (1991) was used to classify the volcanic rocks. As shown in **Figure 19** most of the rocks plot in the basalt field, and just one as foidite that may be related to the high hydrothermal alteration present in that rock. Dikes range from basanite to trachy-dacites. The magmatic series was determined using AFM diagram (**Figure 20**) where dikes (purple points) plot into the calc-alkaline field whereas the basalts (green and blue points) are plotting in the transition between the Kuno, (1968) and the Irvine & Baragar, (1971) lines mainly related to the tholeiitic field.

Harker diagrams for major elements vs. MgO among basalts (**Figure 21)**, are showing that MgO varies between 8 and 13%, there are negative trends on Na_2O, Fe_2O_3, TiO_2 and Al_2O_3 while CaO shows a positive trend and SiO_2 has a flat pattern, there are at least 2 groups of basalts. LOI values (**Figure 22**) for igneous rocks range from 0.97 to 3.55 being dikes the ones with higher values. Only one of the samples (ERML – 012) has an anomalous value of 18.1 due to the degree of alteration this sample is not suitable for geochemical interpretation, black chert has a similar value due to a high content in organic matter as it is confirmed by petrography and XRD analysis. Other sedimentary rocks range from 4.82 to 5.89 for LOI.

4.3.2 Trace and REE elements

Trace and REE elements were used as a complementary classification for volcanic rocks and their tectonic setting (**Figure 23**), they clearly separate two groups for basalts as follow: N-MORB tholeiitic basalts, E-MORB basalts. The dikes belong to the calc-alkaline volcanic arc. (Cabanis and Lecolle, 1989).

To determine the trace and REE elements patterns, the element concentrations were normalized with primitive mantle (Sun and McDonough, 1989) and with chondrite (Nakamura, 1974) respectively (see **Figure 24** and **Figure 25**). Samples are generally enriched in LILE and show a flat pattern in the HFSE with positive anomalies in Li, Sr and Pb (**Figure 24**). The REE spider diagram for basalts (**Figure 25**) are clearly dived into two groups, both have flat patterns however an enriched concentration (10 times in magnitude order) is related to the E-MORB basalt previously discussed. In contrast the dike's pattern has a negative slope from LREE to HREE indicating a possible subduction-related magma (Grunsky and Massey, 1995).

4.4 Geochemical vectors

Basalts were chosen to see geochemical variation starting at 180m to 20m away from the main ore body "Zeus"; there are important increments on MgO up to 14%, Tl up to 2ppm, CCPI (Chlorite Carbonate Pyrite Index) up to 90 and AI (Alteration Index) up to 50 (**Figure 26**) at the contact with the black chert layer. For the alteration box plot (**Figure 27**) hydrothermally altered basalts range from 85 to 95 in CCPI and 40 to 60 in AI, while unaltered samples are between 80 to 85 and 35 to 45 for CCPI and AI respectively.

As shown in **¡Error! No se encuentra el origen de la referencia.** variation profiles across t ransect 1760 made with simple topo to raster interpolation in ArcGIS pro® were used to build

several profiles across the transect at 1760 m.a.s.l (**¡Error! No se encuentra el origen de la referencia.**), and the chemical elements variations and chemical indexes trough the basalts. The CCPI (Chlorite Carbonate Pyrite Index), the AI (Alteration Index) (**Figure 26** a, b) MgO and the Tl (**Figure 26** c, d) exhibit the best results with a big increase close to the Zeus mineralized body. Analysis were restricted to basalts to avoid chemical variations induced by self-lithology. Very low values (ca. 0) in MgO and Tl and high values on CCPI (up to 86) at 80m indicate that there is a clear correlation of the host rock alteration and the related stockworks due to chemical diffusion from basalts to dikes. No clear variations were found in other elements such as Li, Na_2O, Ti, W, Rb, Cs.

5. DISCUSSION

5.1 Tectonic setting and VMS type

When comparing basalts at El Roble mine with the "classic" Barroso basalts described by Rodríguez García and Arango Mejía, (2013) (**Figure 28**), it is possible to see that there is a match between both minor and trace element signatures with the basalts from El Roble area. Nevertheless, those studies are regional, and cover wide areas (Ingeominas et al., 1986; Rodríguez García and Arango Mejía, 2013), thus, differentiation of different types of basalts became sometimes difficult. In this study, litho-geochemistry was done in a small area along 180 lineal meters giving us a detailed resolution.

Geochemical signature of N-MORB is represented by deplation in highly incompatible elements and its origin is associated with domains comprasing an spreading segment of oceanic crust with an uniform low degree of partial melting coming from an homogeneous source (Viereck et al., 1989) wile E-MORB is enriched in highly incompatible elements due possibly because of infiltration of enriched lower mantle materials to the upper mantle, in adition it has

also been sugested that this enrichment could come from metasomatism of ambient upper matle peridodite by low degree patial melts (Arevalo and McDonough, 2010).

Therefore, we can clearly identify two different basalts types, that may turn into different mantle sources: E-MORB and N-MORB-related, induced by a different partial melting (Arevalo and McDonough, 2010). Moreover, the study area is influenced by porphyry dikes that show a typical subduction pattern with ages of 16-17Ma (De Brito et al., 2010) cutting the stratigraphic sequence plus the relationship between Barroso and other intrusive sequences such as Mandé Batholith, which are related with the subduction of the Nazca plate bellow south America (Ingeominas et al., 1986; Redwood, 2019).

Five lithostratigraphic groups of volcanogenic massive sulfide deposits have been reported so far (Franklin et al., 2005; Shanks and Thurston, 2012): (1) bimodal mafic (2) mafic (3) pelite-mafic (4) bimodal felsic and (5) siliciclastic felsic. As we see in El Roble mine, there are pelite-mafic interbedding, including micritic limestones with globose foraminifera (unicameral, bicameral or multilocular) and organic matter (well preserved giving dark color to the rock, in a deep marine anoxic environment), subordinate siltstone, wake and sandstone mafic-ultramafic sill and MORB-like lava flows, like the ones described in the third group above mentioned (Franklin et al., 2005). Moreover, El Roble deposit has layers of basalts forming peperitic contacts with black chert unit.

The succession seen in the stratigraphic column (**Figure 5**b) is common in rifts that are proximal to continental - margins, where the instauration of a subduction zone, induce high rates of continental sedimentation (e.g. Urrao Member of the Penderisco formation). Therefore, given the lithological association and the basalts geochemical signature it is possible to define El Roble deposit as a pelitic - mafic related VMS.

5.2 Geochemical vectors and exploration

As seen in the results there is a clear variation in the chemical composition and texture of basalts, the presence of E-MORB hyaloclastites followed by N-MORB basalts and dike stockworks is a good indicator of the proximity to ore bodies such as Zeus.

Other important indicators of proximity to the main deposit are: (1) the CCPI (Chlorite-carbonate-pyrite-index) measures the increase of MgO and FeO, this happens when maximum hydrothermal temperatures and water/rock ratios are reached, and Mg-Fe chlorite grows (**Figure 26**a) (Large et al., 2001). (2) the Alteration Index (AI) (**Figure 26**b) quantifies chlorite and sericite alteration occurrence because of the sodic plagioclase breakdown and replacement by sericite and chlorite (Ishikawa et al., 1976); values between 50 and 100 represent hydrothermally altered rocks, in El Roble case, the favorable basalts have average values of 84 and 42 for CCPI and AI respectively. In addition, single element variation (MgO and Tl) across the 1760 meters of altitude transect gave the best results, where values of more than 13% and 1ppm respectively, indicate the proximity of around 20m to the ore bodies other elements such as Na_2O that usually has a negative anomaly is close to the ore body (Piercey, 2009), is not conclusive for El Roble deposit because of the overprinted hydrothermal alteration closely related to the Cenozoic arc environment.

6. CONCLUSION

The chemical characteristics of the studied samples are basalts formed in a mid-oceanic ridge environment related to upper mantle affinities (E-MORB and N-MORB); however a generalized arc setting have been proposed for the Barroso Formation (e.g. Rodríguez García and Arango Mejía, 2013; Cetina et al., 2019); thus we propose a combination of arc environment and local basin formation related to a local pull-apart (?) and/or ridge events. Moreover, at the same time the VMS-mineralization may occur. Later intrusions may have happened in an arc environment (De Brito et al., 2010) when the oceanic basalts were accreted to the continental margin (e.g. Mandé Batholith and related dikes).

We have detected at least two different hydrothermal alterations events at El Roble deposit, the first during the formation rift-pull-apart(?) related basalts formation and the induced mineralization due to oceanic water percolating into the rocks. Secondly, an alteration after the accretion of these units to the continent in a subduction-related environment forming stockworks.

Major, minor and trace elements such as Tl, Mg, and alteration indexes such as AI and CCPI are well correlated with the identified basaltic groups (e.g. hyaloclastites, altered basalts, diabases). Both together became clear vectors for future exploration targets at El Roble deposit.

Until now, there is not enough data to build a schematic section with the precise litho-geochemistry variation. Also, deformation and stratigraphy are not well understood in the study area; however, it plays an important role in understanding the geology and ore deposition. Thus, detailed studies such as micro-structural analysis, complemented with analysis of magnetic anisotropy, detrital and basalts dating, dense mineral studies, detailed palynological and fossil characterization, field structural data collecting and modelling, conglomerate petrography, S

and O isotopes and a wider sampling for total rock geochemistry, together with thin and polished sections petrography are the future challenges to get a full understanding of the emplacement and formation of the basin and the deposit. Therefore, this work is the first approach to a much bigger work that will be done in the next few years.

ACKNOWLEDGEMENTS

To Atico Minig corporation and MINER S.A for providing all the information and resources to conduct this investigation. Gmas Lab in Bogotá for providing human and technical resources to perform petrography and XRD analysis.

7. REFERENCES

ALS, 2020a, ALS Certificate MD20096795.:

ALS, 2020b, Four Acid Digest & Technology Advanced ICP-MS Providing robust datasets for use in Lithogeochemical Mapping.:

ALS, 2020c, Schedule of services & fees; Geochemistry.:

Álvarez, E., and González, H., 1978, Geología y geoquímica del Cuadrángulo I-7 (Urrao) Mapa escala 1:100.000.:

Alvarez, J., 1971, Informe preliminar sobre geoquímica de la Cordillera Occidental.:

Arevalo, R., and McDonough, W. F., 2010, Chemical variations and regional diversity observed in MORB: Chemical Geology, v. 271, p. 70–85.

Atico Mining, 2020, El Roble Mine, (http://aticomining.com/projects/el-roble-mine/snapshot/).

Le Bas, M. ., and Streckeisen, A. ., 1991, The IUGS systematics of igneous rocks: Journal of the Geological Society, v. 148, p. 825–833.

Bas, M. J., Maitre, R. W., Streckeisen, A., and Zanettin, B., 1986, A Chemical Classification of Volcanic Rocks Based on the Total Alkali-Silica Diagram: Journal of Petrology, v. 27, p. 745–750.

Batiza, R., and White, J. D. L., 2007, Submarine lavas and hyaloclastite, in Encyclopedia of volcanoes.:

De Brito, R., Mejía, P., Ordoñez, O., Vasconcelos, P., Brilhante, J., and Bijos, S., 2010, 40Ar/39Ar and U-Pb LA-ICPMS dating and the tectonic significance of andesitic porphyry dykes from the El Roble Cu-Au VMS deposit, Eastern Cordillera, Colombia, in VII SSAGI South American Symposium on Isotope Geology Brasília: Brasilia.

Cabanis, and Lecolle, 1989, Tectonic classification of mafic igneous rocks:

Cediel, F., and Shaw, R. P., 2019, Geology and Tectonics of Northwestern South America (F.

Cediel & R. P. Shaw, Eds.): Frontiers in Earth Sciences, Cham, Springer International Publishing, 1010 p.

Cetina, L. M., Tassinari, C. C., Rodríguez, G., and Correa-Restrepo, T., 2019, Origin of pre-mesozoic xenocrystic zircons in cretaceous sub-volcanic rocks of the northern Andes (Colombia): paleogeographic implications for the region: Journal of South American Earth Sciences, v. 96.

Espada, E., 2012, EL ROBLE VMS CU-AU BELT CHOCÓ DEPARTMENT, COLOMBIA STRUCTURAL SETTING & EXPLORATION IMPLICATIONS.:

Etayo, F., González, H., and Álvarez, J., 1980, Med Albian ammonites from northern Western Cordillera, Colombia: Geología Norandina, v. 2, p. 25–30.

Franklin, J. M., Gibson, H. L., Jonasson, I. R., and Galley, A. G., 2005, Volcanogenic Massive Sulfide Deposits, in One Hundredth Anniversary Volume: Society of Economic Geologists, p. 523–560.

Gill, R., 2010, Igenous rocks and processes: Wiley-Blackwell, 472 p.

Gmas, 2020, Procedimientos Petrografía.:

Grunsky, E., and Massey, N., 1995, Using geochemical data: Evaluation, presentation, interpretation: Computers & Geosciences, v. 21, p. 439–441.

Ingeominas, Calle, B., and Salinas, R., 1986, Geología y geoquímica de la plancha 165 carmen de atrato escala 1:100.000 memoria explicativa.:

Irvine, T. N., and Baragar, W. R. A., 1971, A Guide to the Chemical Classification of the Common Volcanic Rocks: Canadian Journal of Earth Sciences, v. 8, p. 523–548.

Kuno, H., 1968, Differenciation of basalt magma: Interscience, p. 623–688.

Large, R. R., Gemmell, J. B., Paulick, H., and Huston, D. L., 2001, The Alteration Box Plot: A Simple Approach toUnderstanding the Relationship between Alteration Mineralogy andLithogeochemistry Associated with Volcanic-Hosted Massive Sulfide Deposits:

Economic Geology, v. 96, p. 957–971.

Nakamura, N., 1974, Determination of REE, Ba, Fe, Mg, Na and K in carbonaceous and ordinary chondrites: Geochimica et Cosmochimica Acta, v. 38, p. 757–775.

Nesse, W. D., 1986, Introduction to Optical Mineralogy.:

Pardo-Trujillo, A., Cardona, A., Giraldo, A. S., León, S., Vallejo, D. F., Trejos-Tamayo, R., Plata, A., Ceballos, J., Echeverri, S., Barbosa-Espitia, A., Slattery, J., Salazar-Ríos, A., Botello, G. E., Celis, S. A., et al., 2020, Sedimentary record of the Cretaceous–Paleocene arc–continent collision in the northwestern Colombian Andes: Insights from stratigraphic and provenance constraints: Sedimentary Geology, v. 401, p. 105627.

Piercey, S. J., 2009, Lithogeochemistry of volcanic rocks associated with volcanogenic massive sulphide deposits and applications to exploration. In Submarine Volcanism and Mineralization: Modern through Ancient: Submarine Volcanism and Mineralisation: Modern through Ancient, p. 15–40.

Redwood, S. D., 2019, The geology of the Panama-Chocó Arc, in Cediel, F. and Shaw, R. P. eds., Geology and tectonics of Northwestern South America: Springer, p. 901–925.

Rodríguez García, G., and Arango Mejía, M., 2013, Formación Barroso: Arco volcánico toleitico y Diabasas de San José de Urama: Un prisma acrecionario T-Morb en el segmento norte de la Cordillera Occidental de Colombia: Boletín de Ciencias de la Tierra, p. 17–38.

Shanks, W. ., and Thurston, R., 2012, Volcanogenic Massive Sulfide Ocurrence Model:, accessed at https://pubs.usgs.gov/sir/2010/5070/c/.

Sun, S. S., and McDonough, W. F., 1989, Chemical and isotopic systematics of oceanic basalts: Implications for mantle composition and processes: Geological Society Special Publication, v. 42, p. 313–345.

Viereck, L. G., Flower, M. F. J., Hertogen, J., Schmincke, H. U., and Jenner, G. A., 1989, The

genesis and significance of N-MORB sub-types: Contributions to Mineralogy and Petrology, v. 102, p. 112–126.

Villagómez, D., Spikings, R., Magna, T., Kammer, A., Winkler, W., and Beltrán, A., 2011, Geochronology, geochemistry and tectonic evolution of the Western and Central cordilleras of Colombia: Lithos, v. 125, p. 875–896.

White, J. D. L., McPhie, J., and Skilling, I., 2000, Peperite: a useful genetic term: Bulletin of Volcanology, v. 62, p. 65–66.

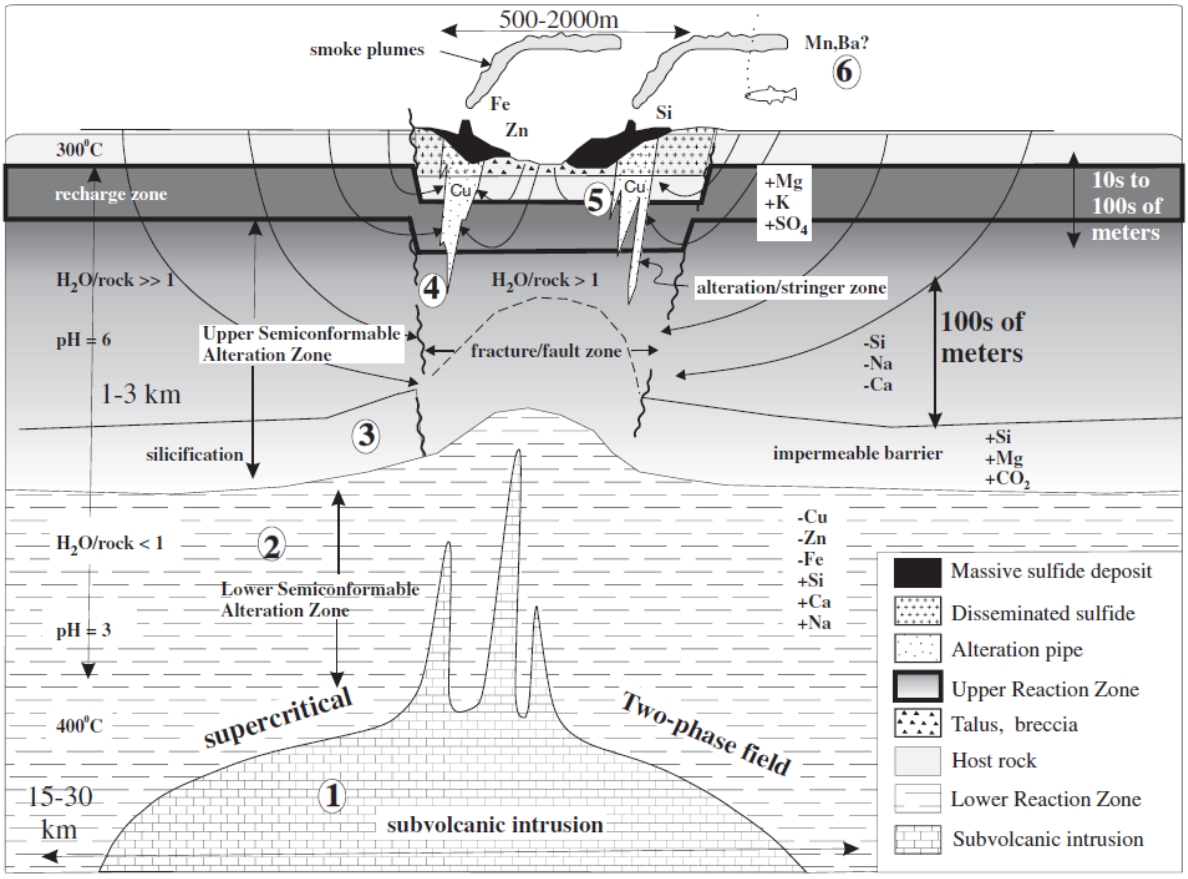

Figure 1. VMS generalized formation model (Franklin et al., 2005).

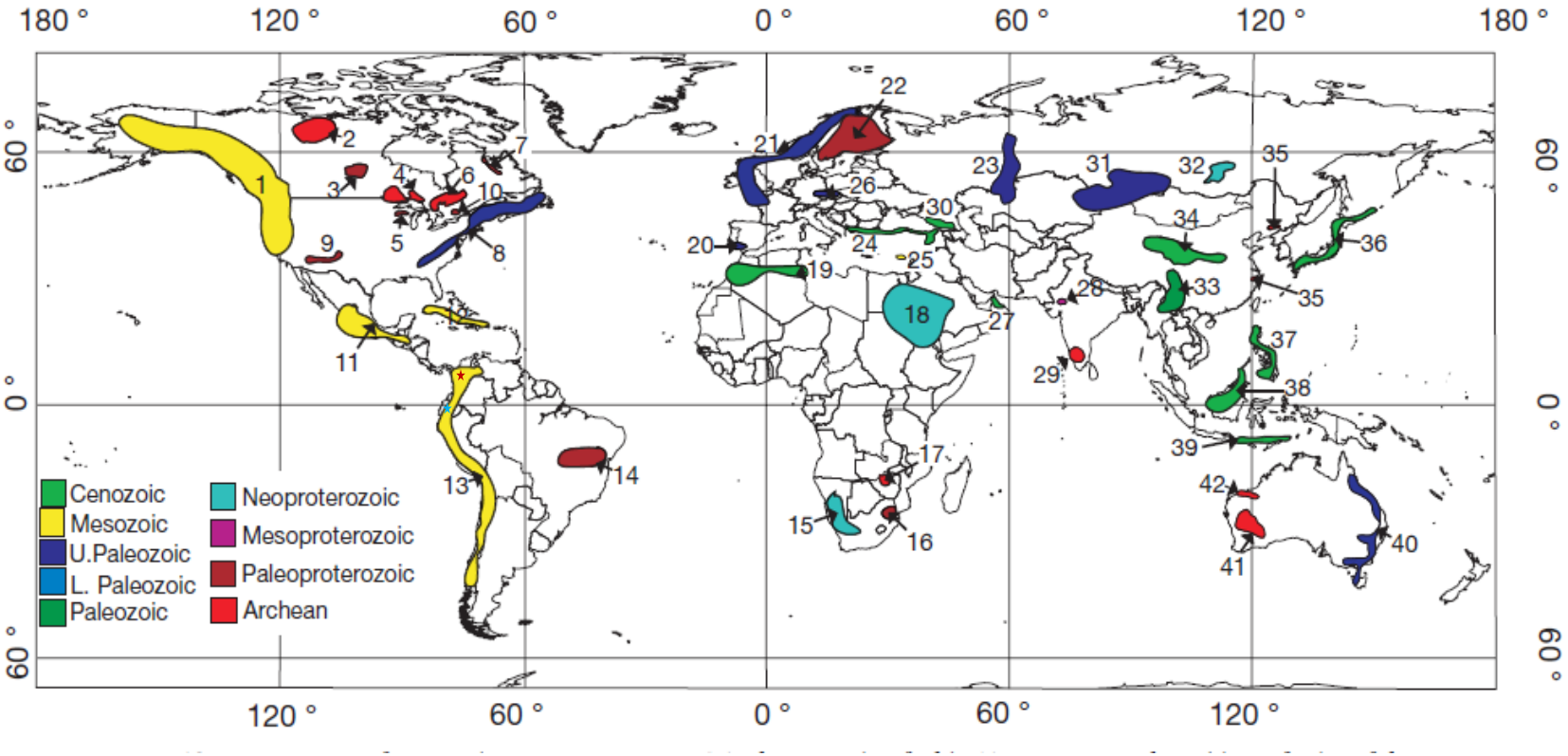
180 °
120 °
60 °
0 °
60 °
120 °
180 °
60 °
0 °
60 °
120 °
60 °
0 °
60 °
120 °
Cenozoic
Mesozoic
U.Paleozoic
L. Paleozoic
Paleozoic
Neoproterozoic
Mesoproterozoic
Paleoproterozoic
Archean
1
2
3
4
5
6
7
8
9
10
11
13
14
15
16
17
18
19
20
21
22
23
24
25
26
27
28
29
30
31
32
33
34
35
36
37
38
39
40
41
42

Figure 2.

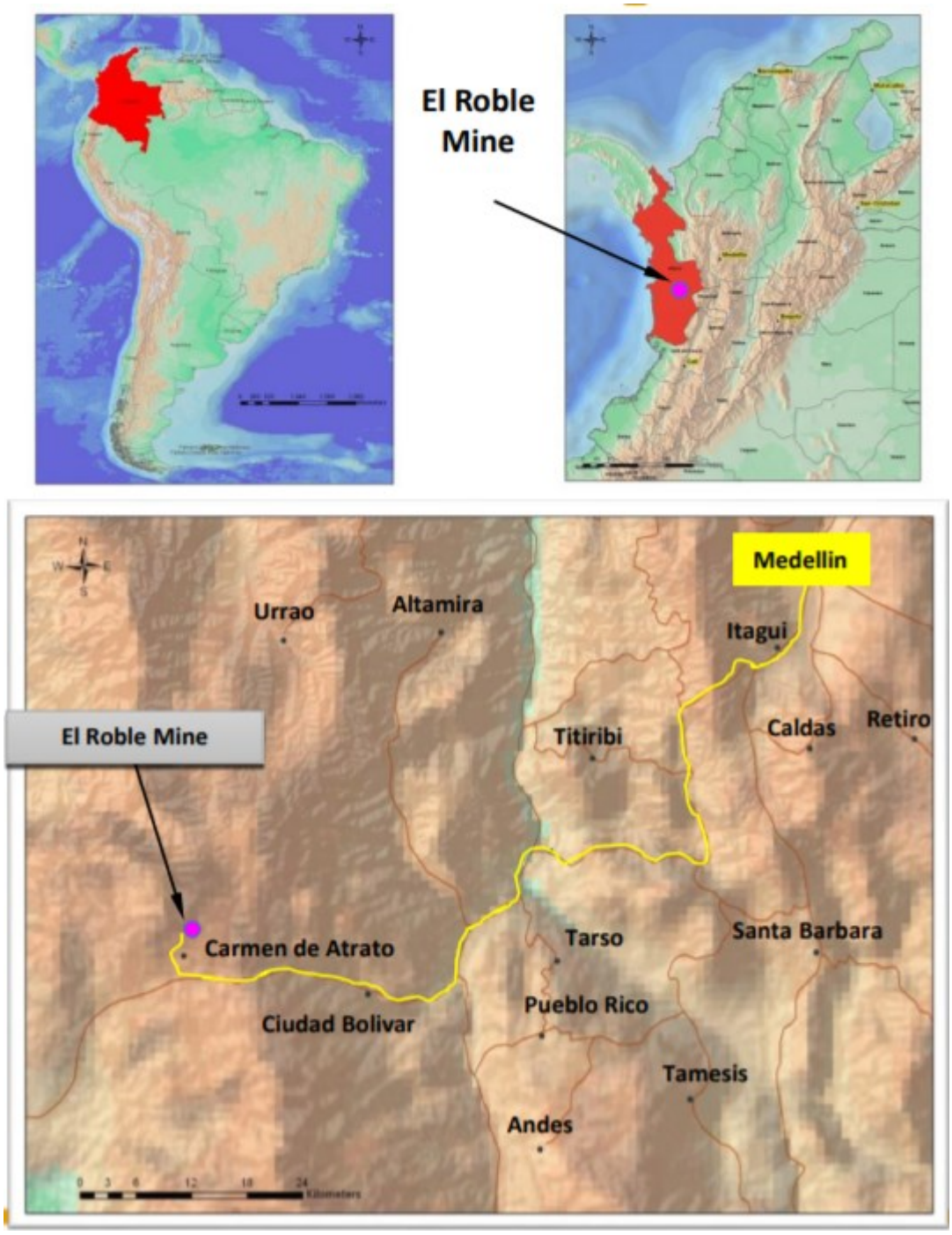

Figure 3. Location of El Carmen de Atrato and El Roble Mine (Atico Mining, 2020).

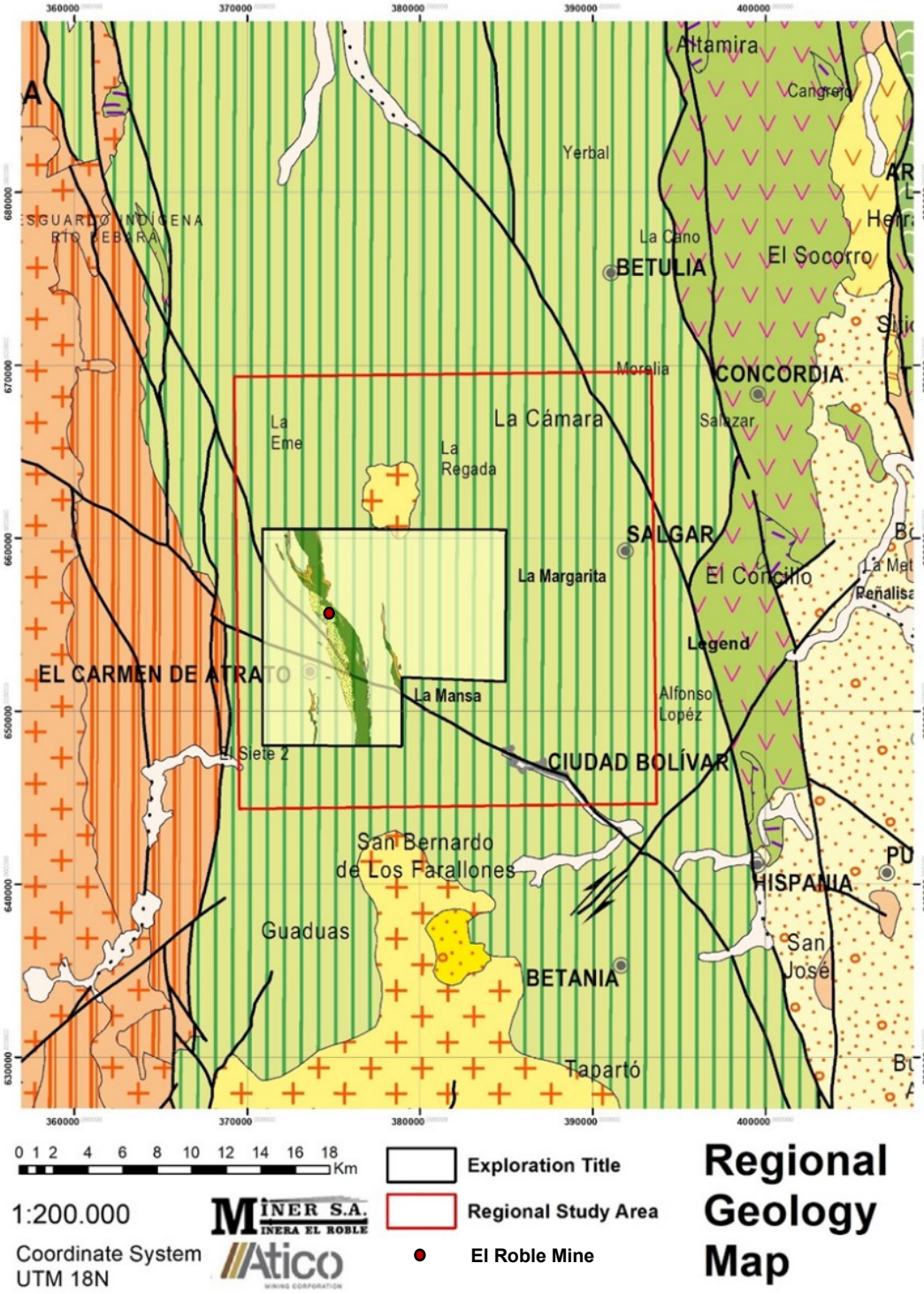

Figure 4. Project localization and regional geology map taken and modified from (Ingeominas et al., 1986).

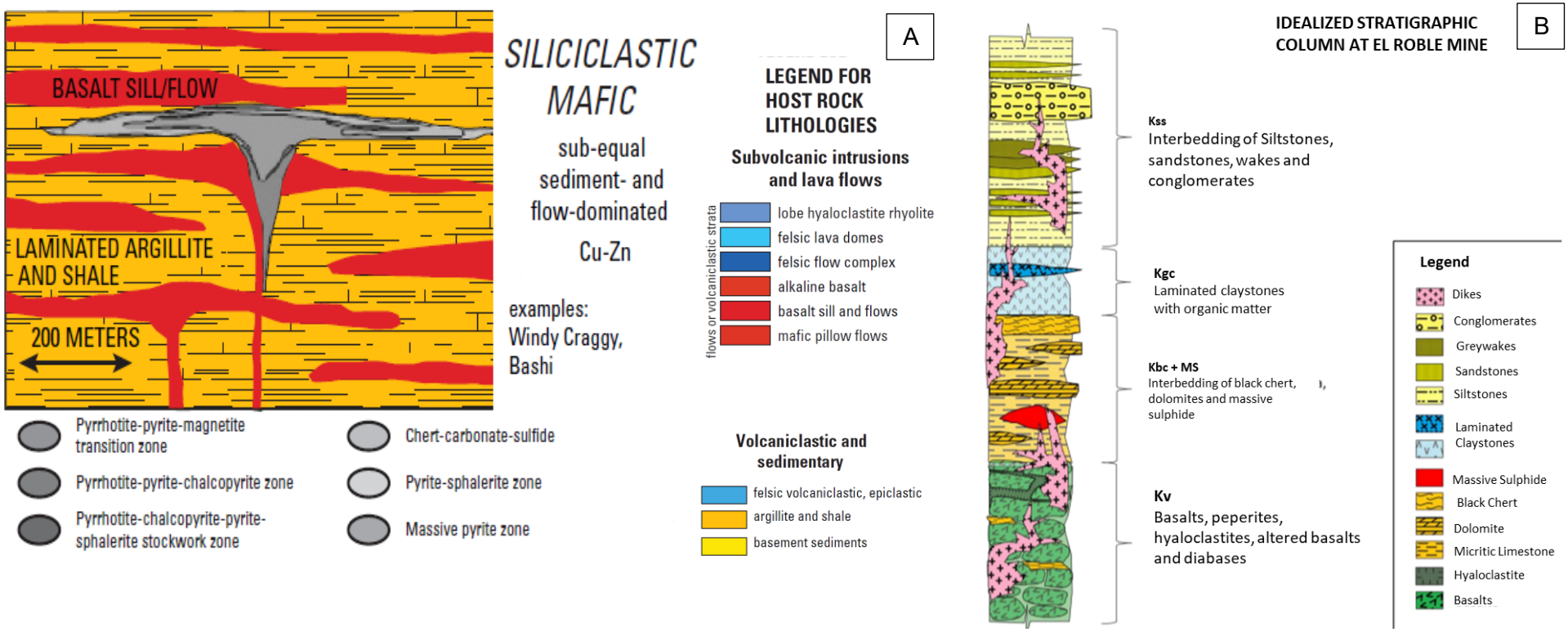

Figure 5. Comparison between (A) Idealized siliciclastic mafic deposit (Taken and modified from Shanks and Thurston, 2012) and (B) idealized stratigraphic column of El Roble mine area, where the lithological association from el Roble can be correlated with the idealized siliciclastic mafic deposit lithological association.

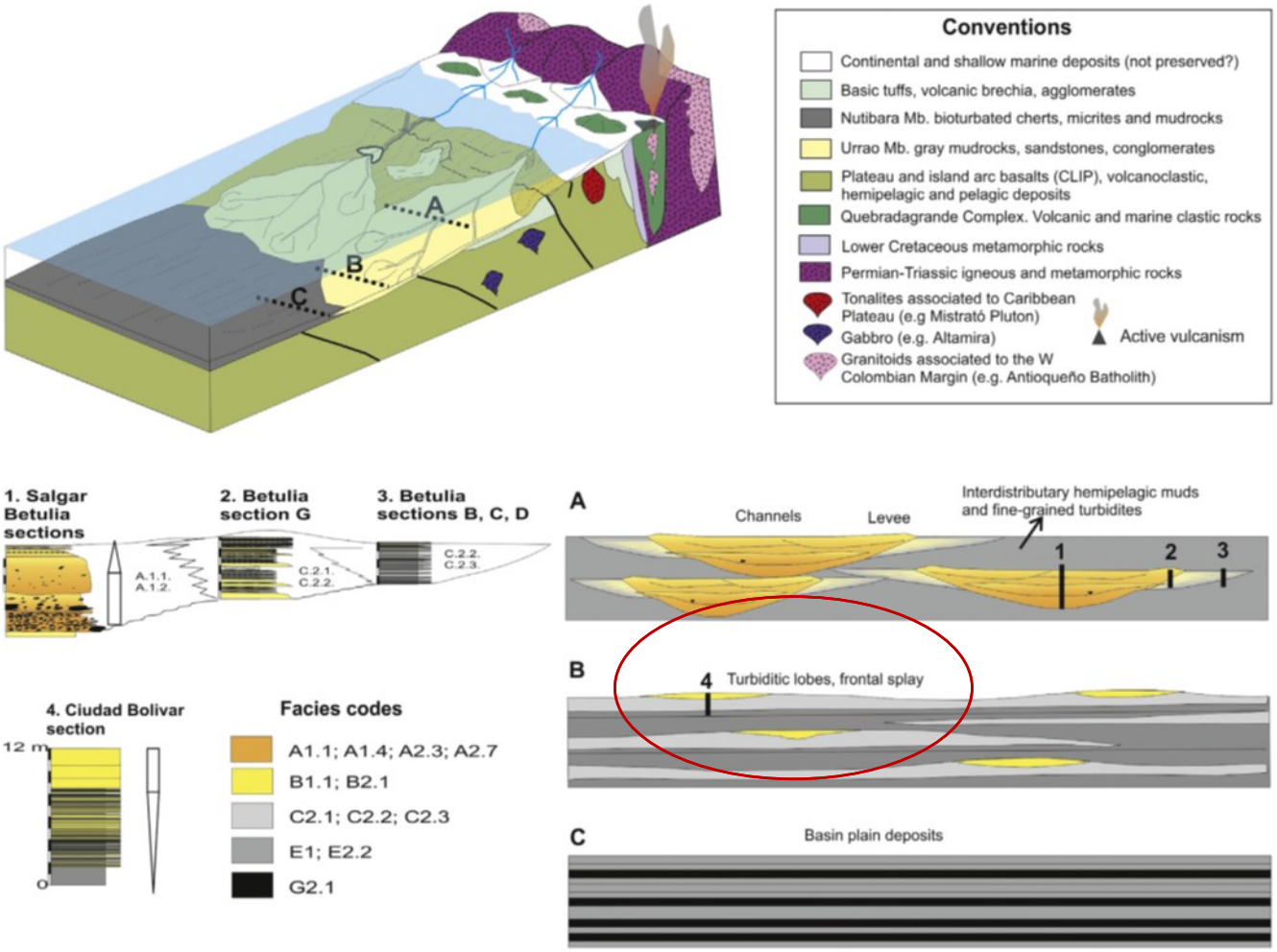

Figure 6. Taken and modified from (Pardo-Trujillo et al., 2020). Red circle is the closest section to the study area it is (B) turbiditic lobe and splay association. Other depositional environment (A) is channel facies and (C) basin plain deposits. Figure is describing Urrao Member of the Pederisco formation depositional setting.

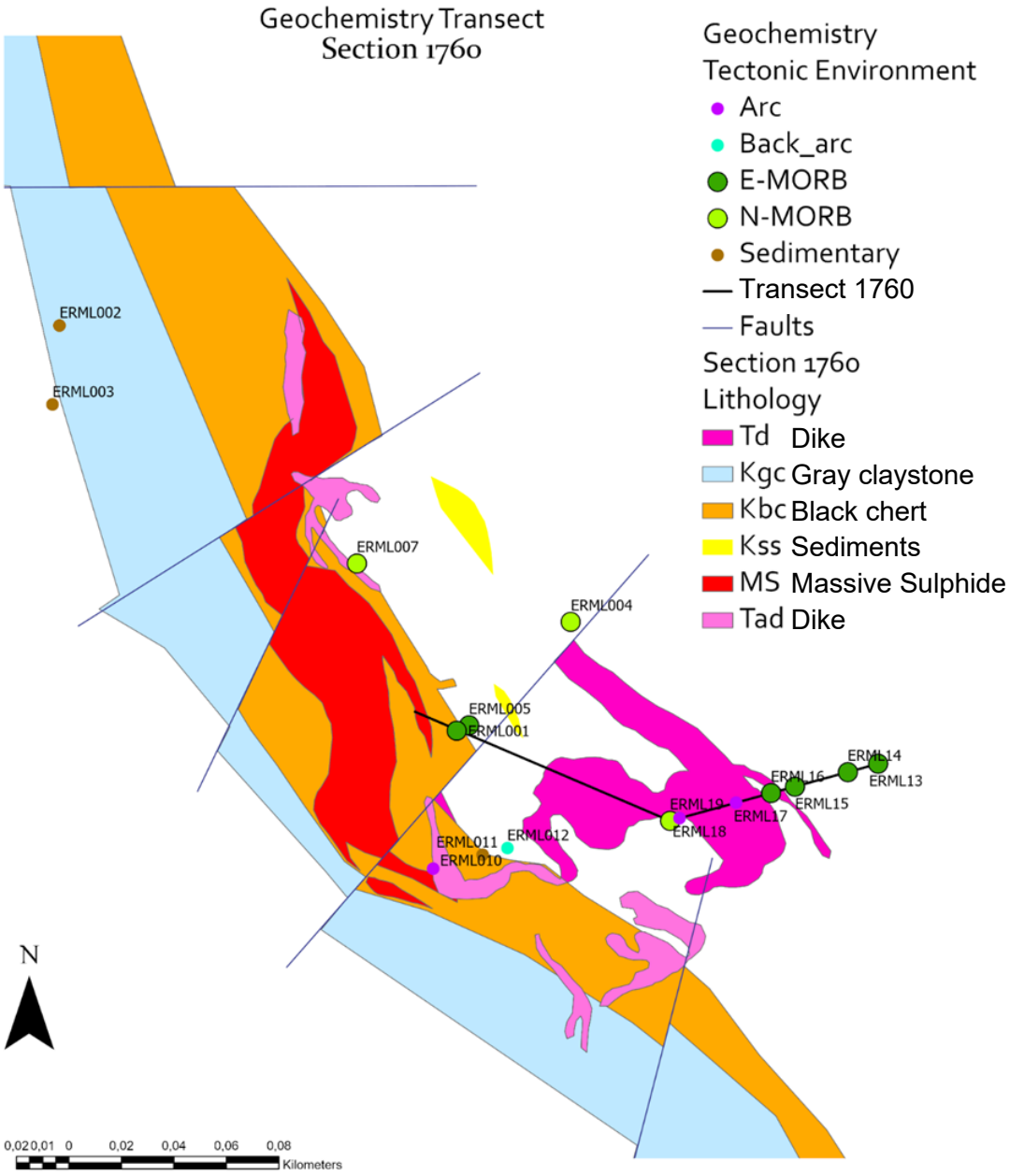

Figure 7. 1760 slide showing in red mineralized body Zeus, Kgc gray claystone, Kbc, black chert and Tad dikes. At the right side of the image there are basalts and at the left side there are sediments as shown in the green and brown points, respectively.

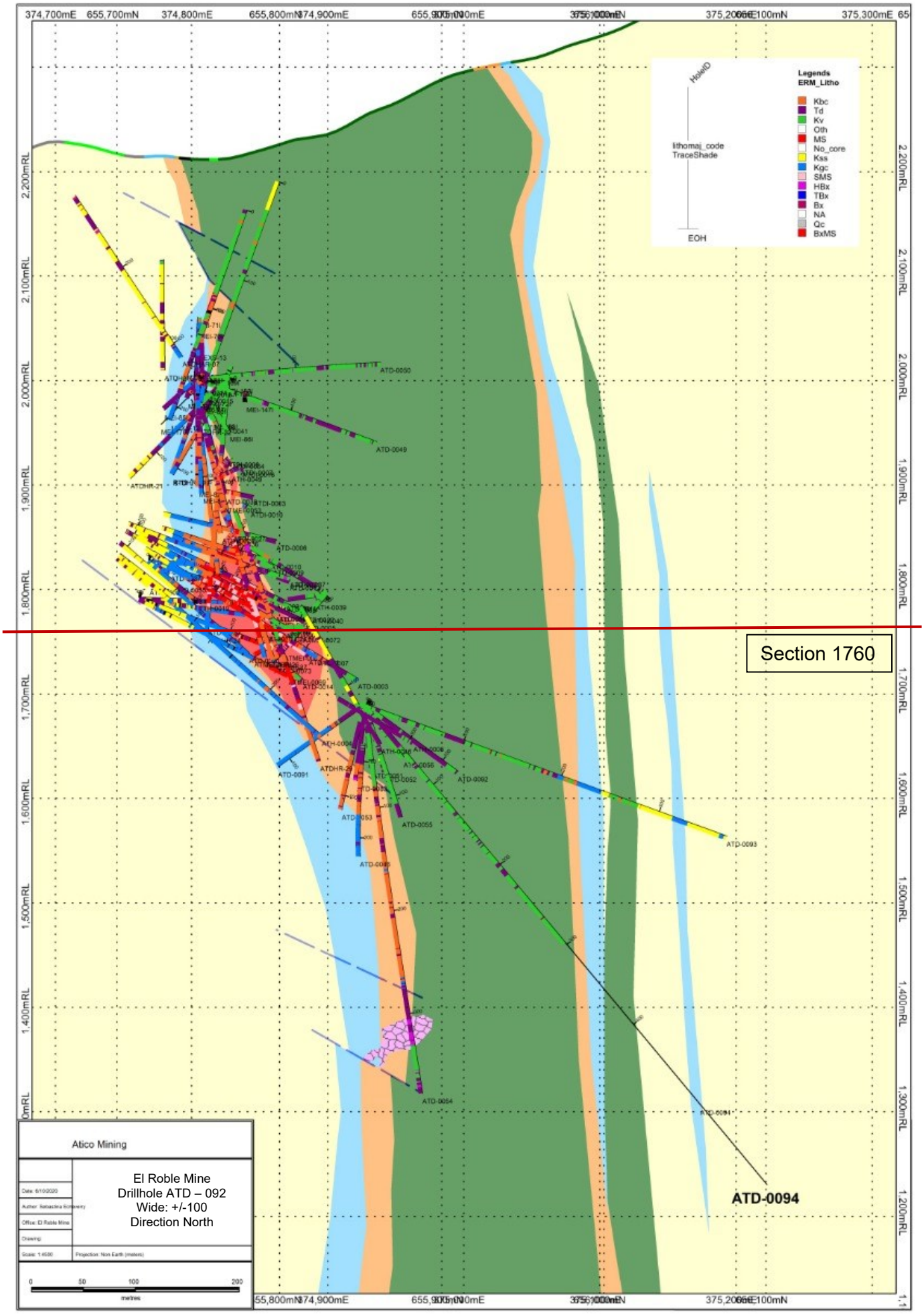

Figure 8. Detailed geological section of El Roble ore bodies and associated lithologies, Penderisco and Barroso formations. With drillholes.

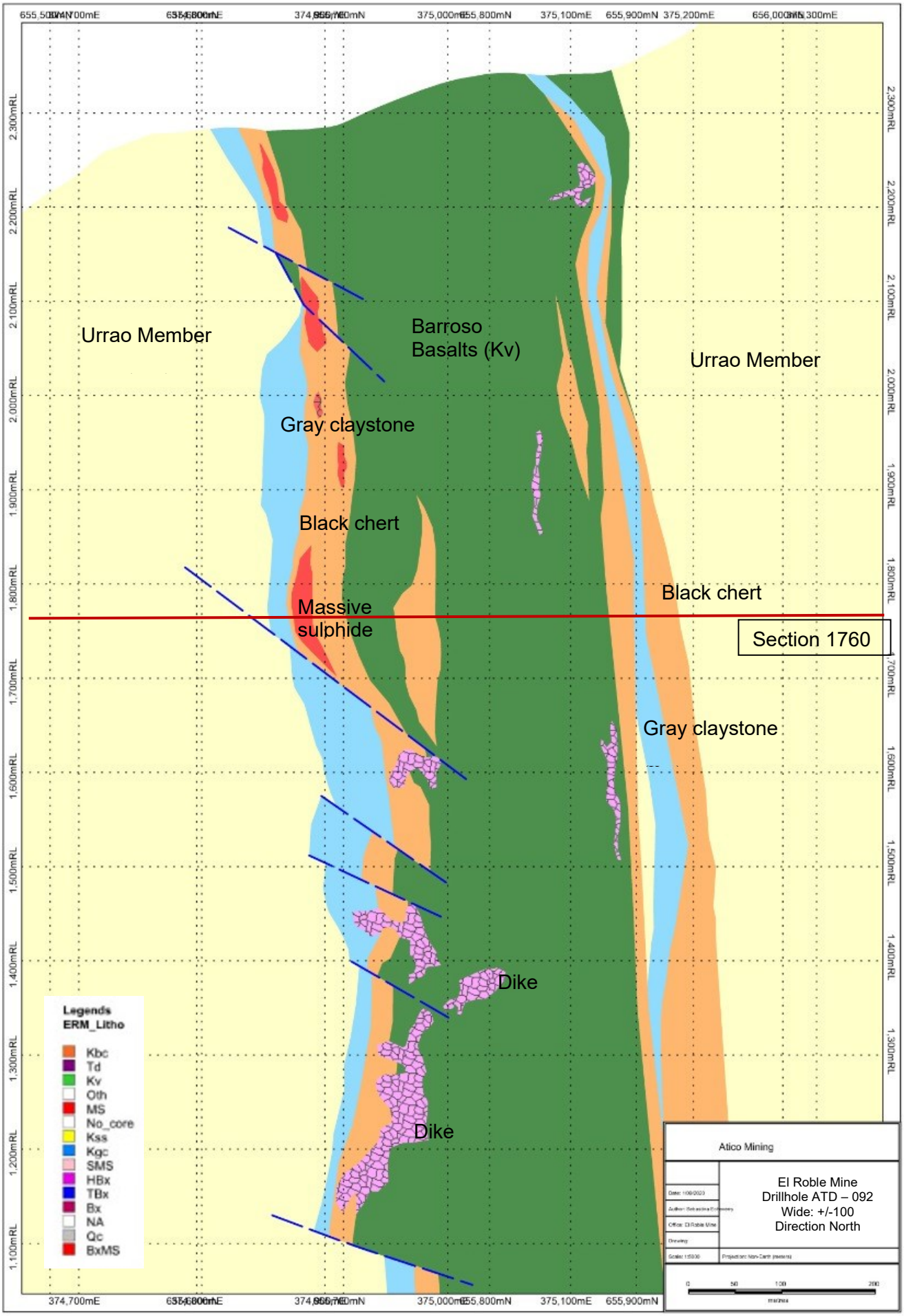

Figure 9. Detailed geological section of El Roble ore bodies and associated lithologies, Penderisco and Barroso formations.

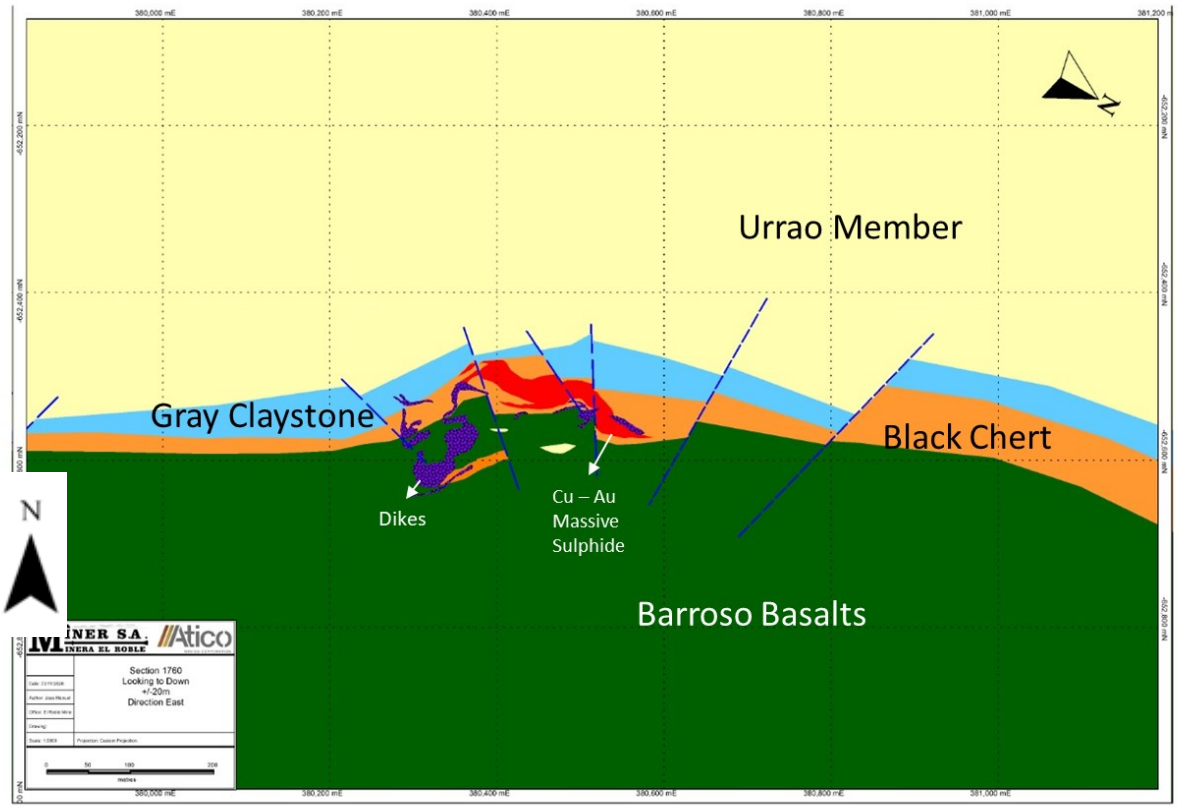

Figure 10. Section 1760 (rotated 125°) and vertical section looking north at Zeus ore body.

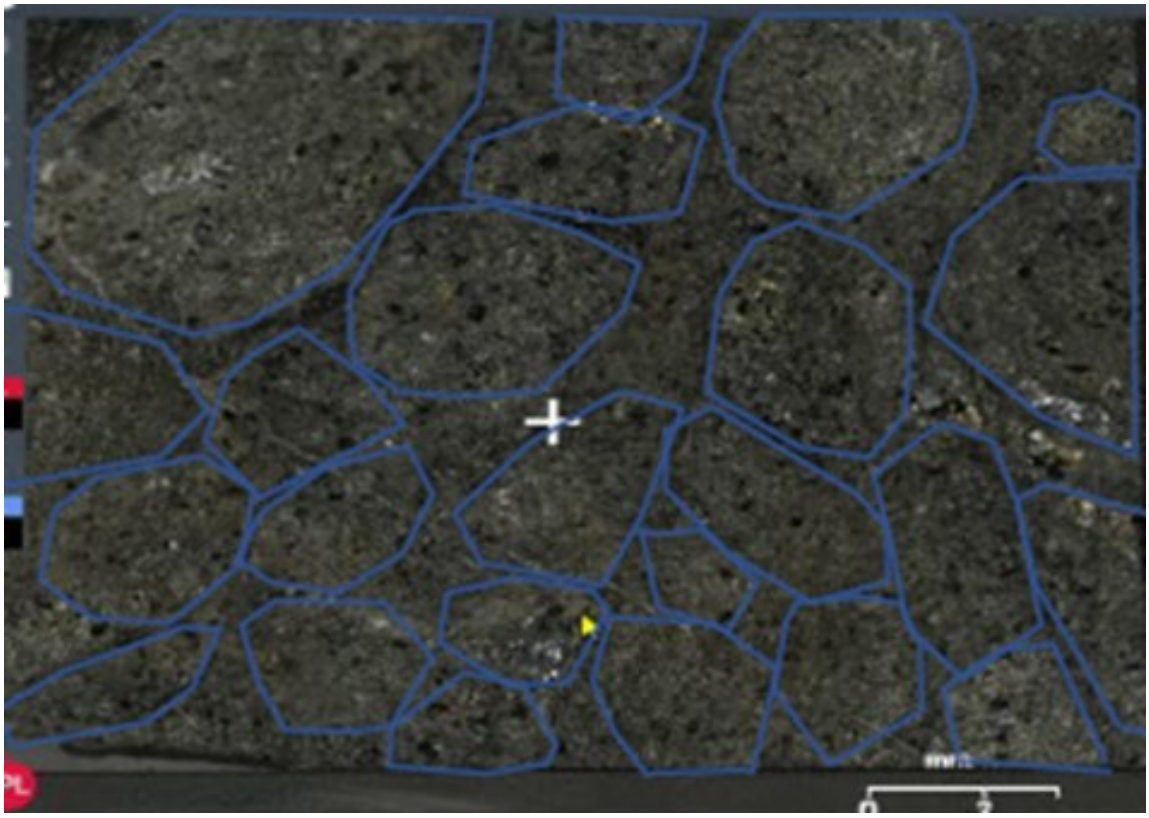

Figure 11. Blue polygons are bounding rock fragments, indicating this is a pyroclastic rock formed during the contact of lava with sea water at the ocean floor. Longitude of the picture 32mm.

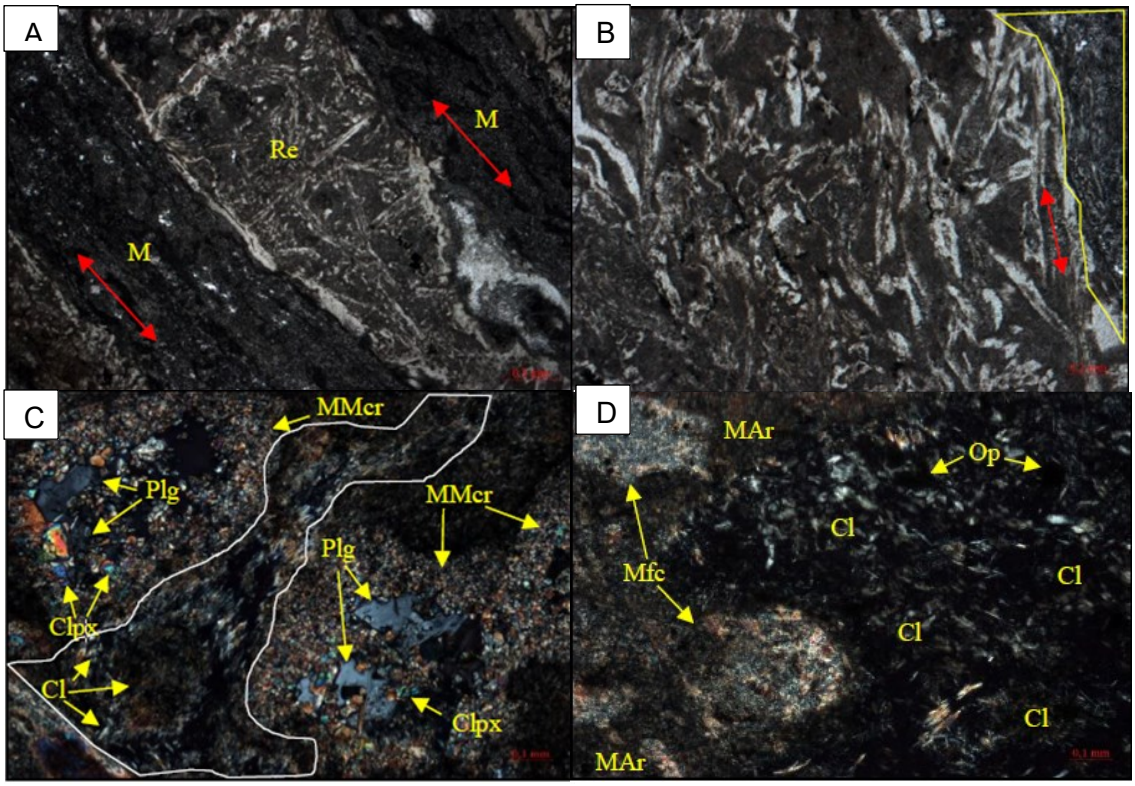

Figure 12. (A) Re corresponds to the host rock and M corresponds to the mineralization, red arrows are indicating the direction of the mineralization forming a reticular setting. Longitude of the picture 5.2mm. (B) Different textures of relict crystals embedded in a fine matrix. Texture could be trachytic; dyke mineralization is bounded by the yellow polygon. Longitude of the picture 2.5mm. (C) Detail of the reticular mineralization. White polygon is showing a mass of clays and chlorite with fibrous – acicular habit. Plg and Clpx are interdigitated plagioclase and clinopyroxene. MMcr is the micro-phenocrysts matrix. Longitude of the picture 2.5mm. (D) Cl chlorite and Mfc micro-phenocrystals altered to clay minerals. Longitude of the image 1.3mm.

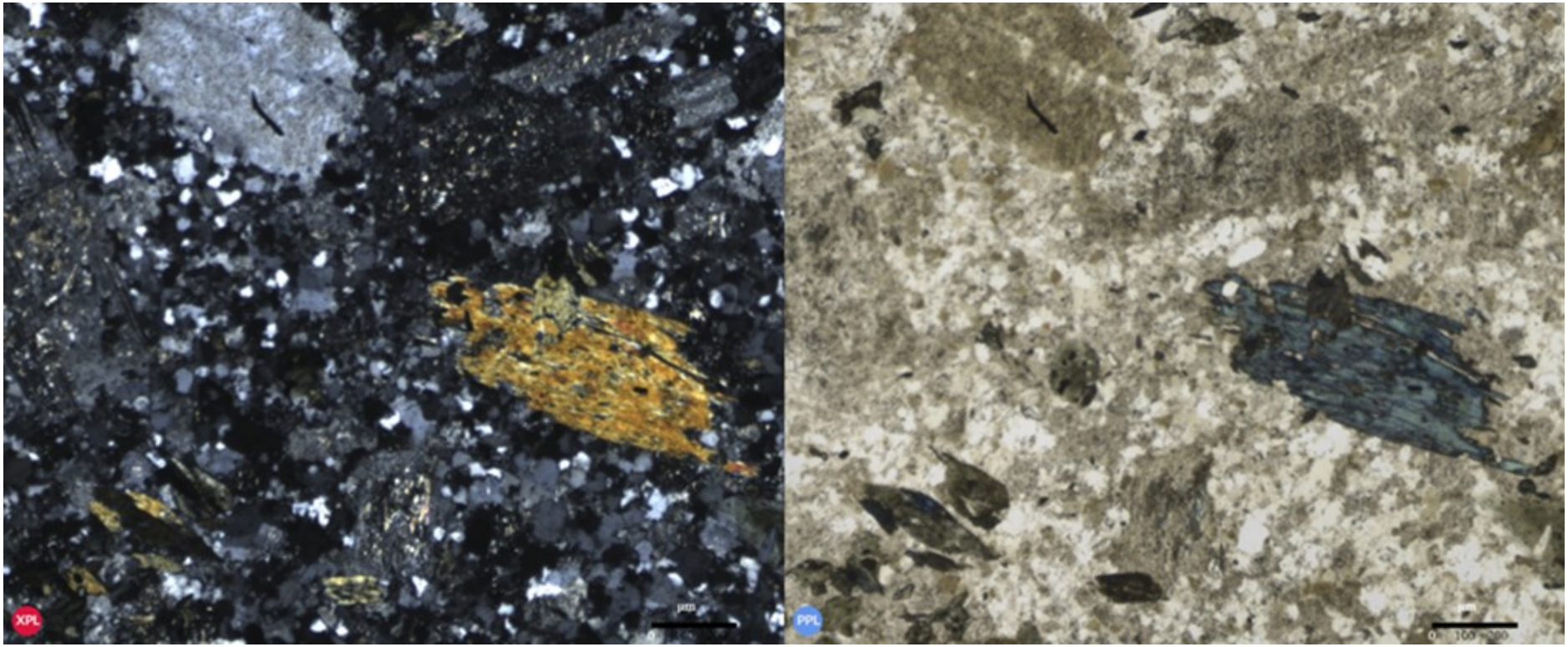

Figure 13. XPL and PPL picture of the dacite showing amphibole with blue pleochroism and plagioclase phenocrysts embedded in a matrix of quartz and plagioclase. Longitude of the picture 5.2mm.

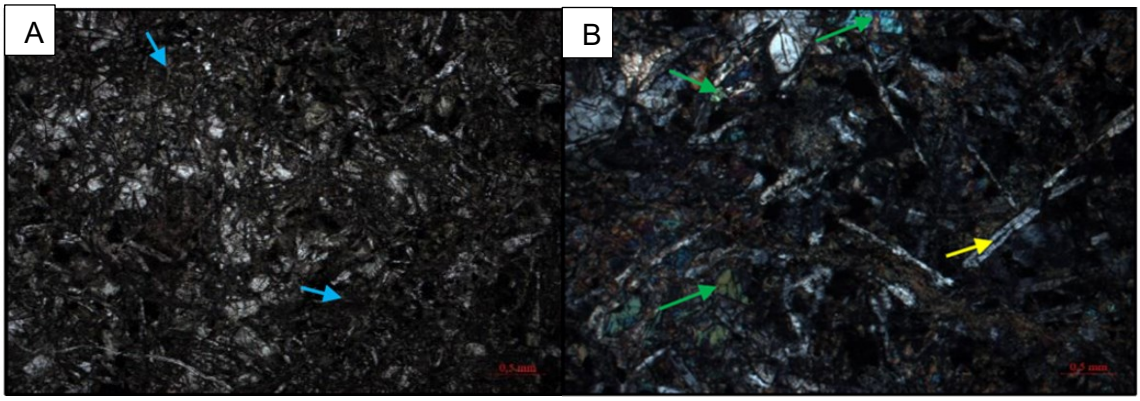

Figure 14. (A) Clinopyroxene (determined by XRD) matrix partially altered (XRD) (Blue arrows). Longitude of the picture 5.2mm. (B) Green arrows augite phenocrystals and yellow arrows are plagioclase crystals. Longitude of the picture 5.2mm.

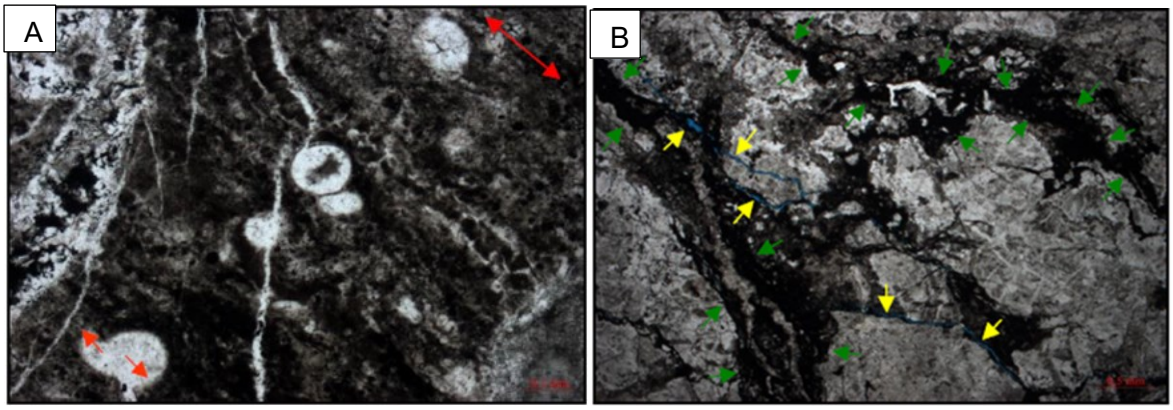

Figure 15. (A) Foraminifera with their cavities occluded with mega quartz, the shell is dislocated by a micro-fault, bioclasts are orientated according to stratification. Longitude of the picture 1.3mm. (B) Example of styloliths (green arrows). Irregular fractures representing porosity (yellow arrows). Longitude of the image 5.2mm.

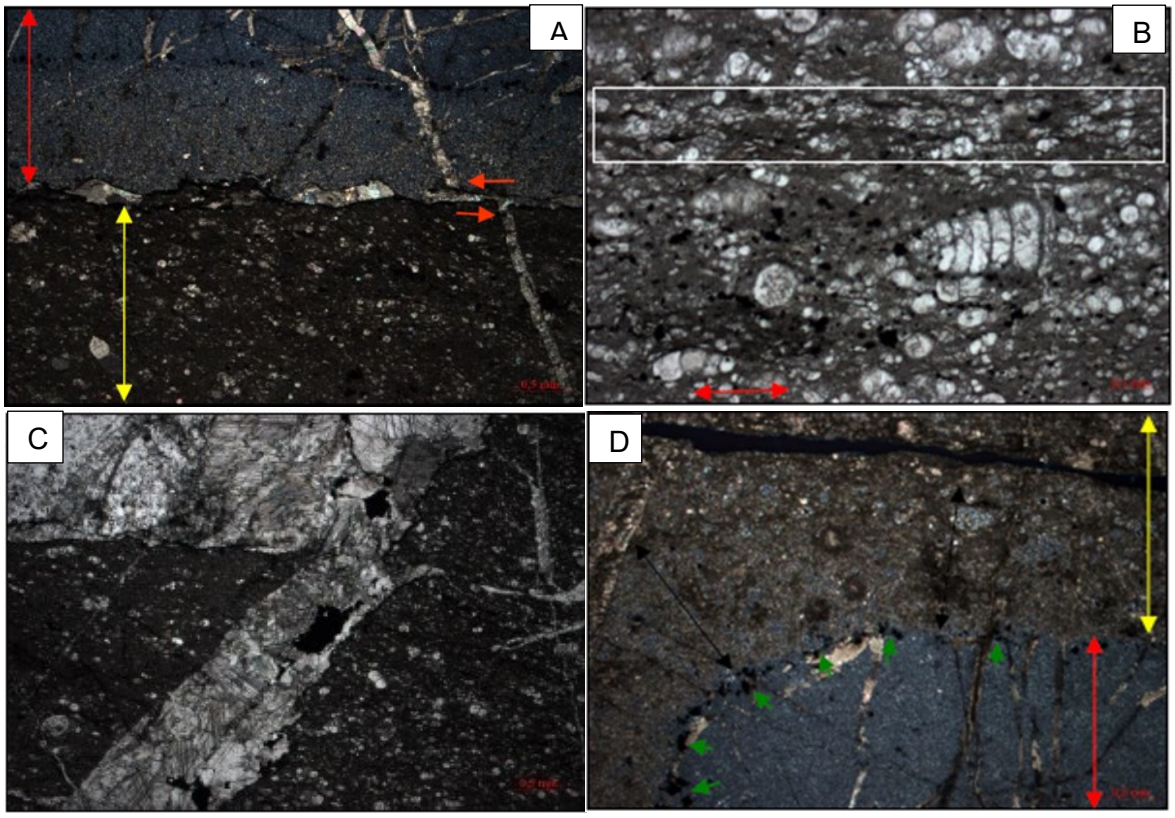

Figure 16. (A) Contact between chert (red arrow) and limestone (yellow arrow). A calcite vein is dissected and displaced by shear deformation (orange arrows) and its displacement produced a stylolite. Longitude of the picture 5.2mm. (B) Detail of calcareous foraminifera floating in micrite parallel to stratification (red arrow) or forming agglomerates (white box). Longitude of the picture 5.2mm. (C) Subvertical thick and thin veins cutting each other composed by calcite and dolomite in less proportion. Longitude of the picture 5.2mm. (D) Contact between limestone (yellow arrow) and chert (red arrow), chert layer is lenticular and discontinuous. Contact between both layers is gradational- Pyrite (green arrows) is surrounding the contact between limestone and chert. Longitude of the picture 5.2mm.

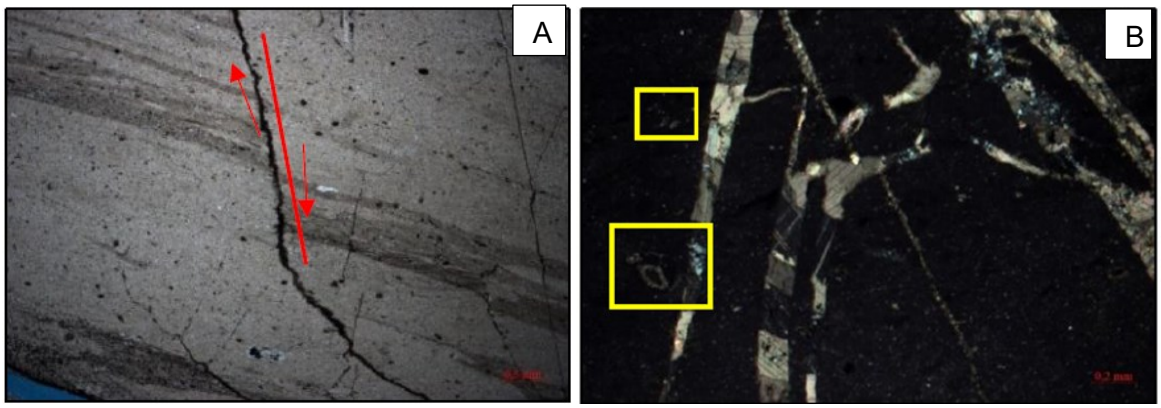

Figure 17. (A) Displacement of the stylolithic surfaces of the micro-faults filled with opaque minerals and organic matter. Longitude of the picture 5.2mm. (B) Agglutinant foraminifera in the yellow boxes. Longitude of the picture 5.2mm.

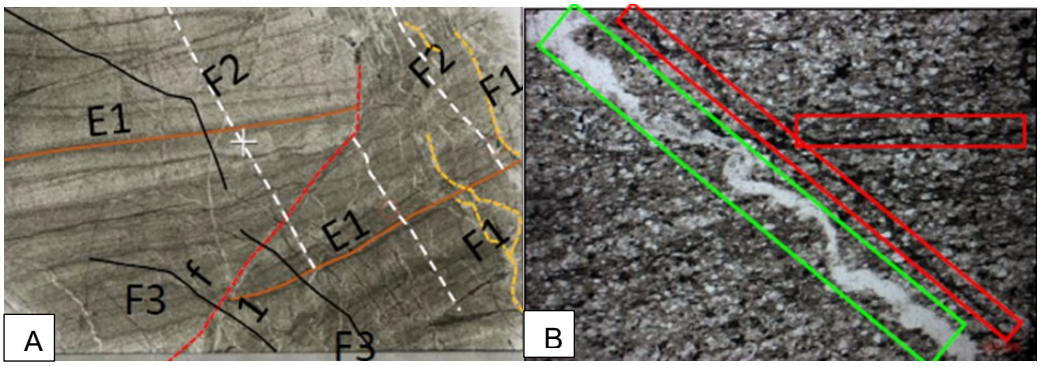

Figure 18. (A) Brown line is showing bedding, other colored lines are showing micro-faults. f1 fault is a syndepositional fault that ends with a cavity filled with dolomite. F1 dashed lines are fractures filled with quartz and siderite, they correspond to a synsedimentary deformation before lithification. Fractures F2 in dashed lines with straight trajectories were formed after the rock was lithified. Fractures F3 have a circular trajectory and are filled with opaque minerals. Longitude of the picture 32mm. (B) stylolithic surfaces filled with quartz (green box) and filled with organic matter (red boxes). Longitude of the picture 5.2mm.

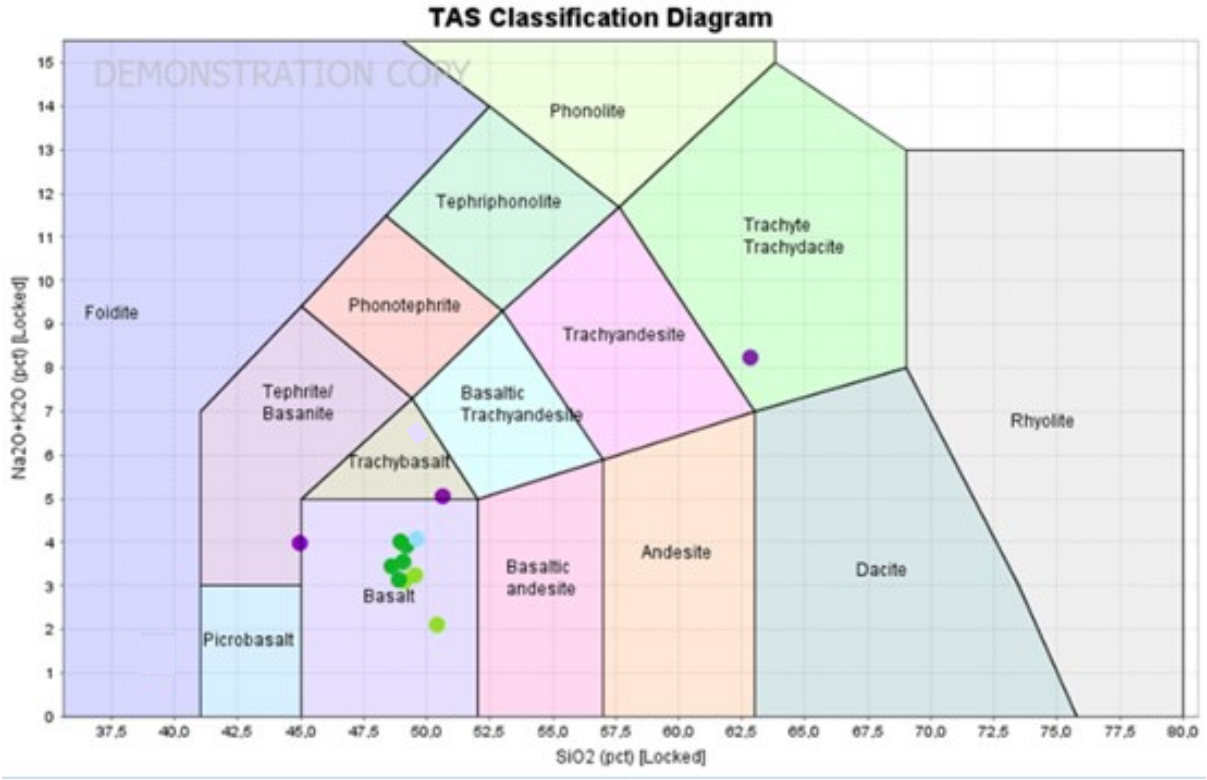

Figure 19. The total alkali-silica (TAS) diagram (Bas et al., 1986). Classification igneous rocks at El Roble mine. Purple points correspond to dikes, dark green correspond to E-MORB basalts, light green correspond to N-MORB basalts.

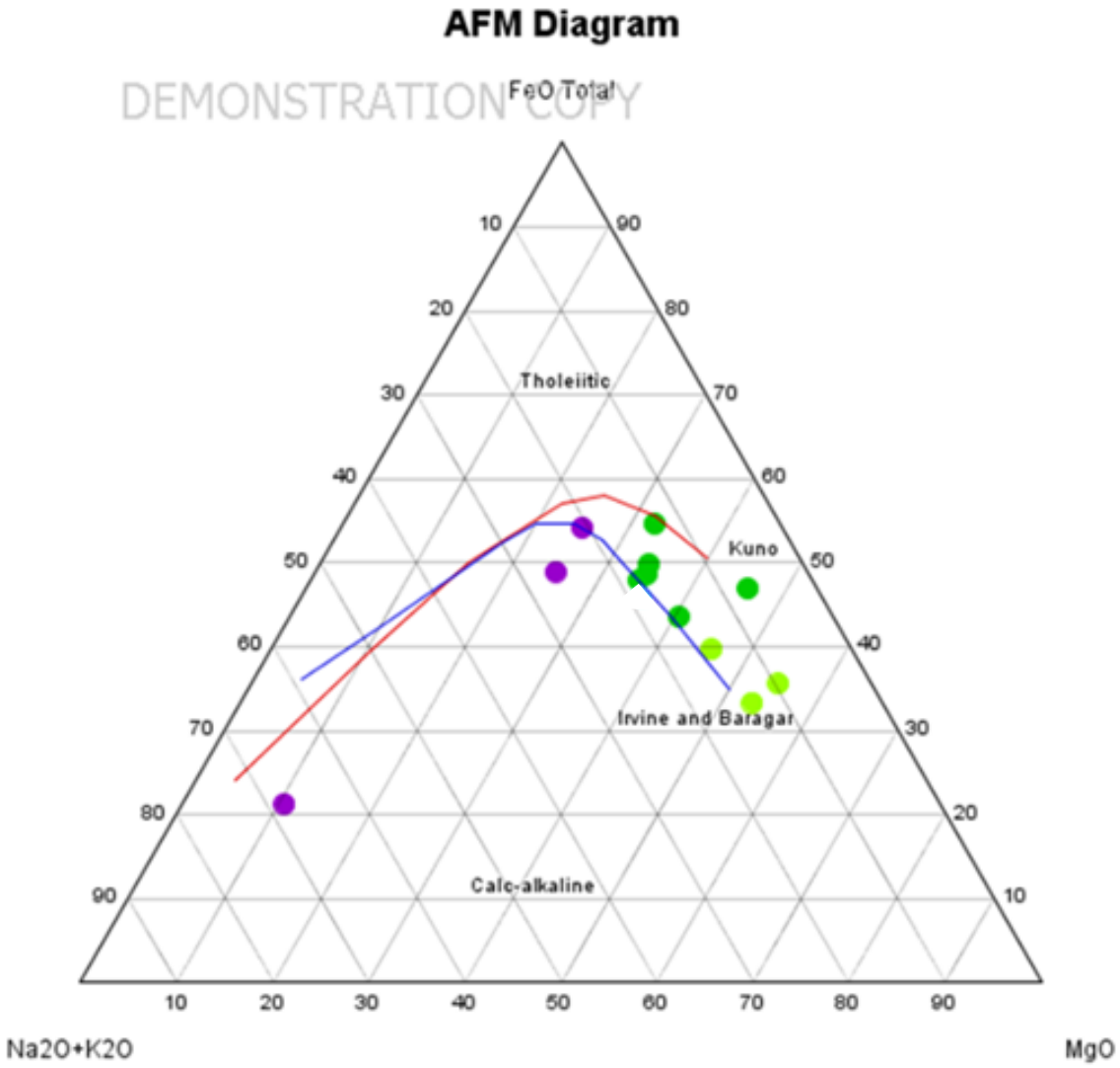

Figure 20. AFM diagram (Kuno, 1968) and (Irvine and Baragar, 1971). Purple points correspond to dikes, dark green correspond to E-MORB basalts, light green correspond to N-MORB basalts.

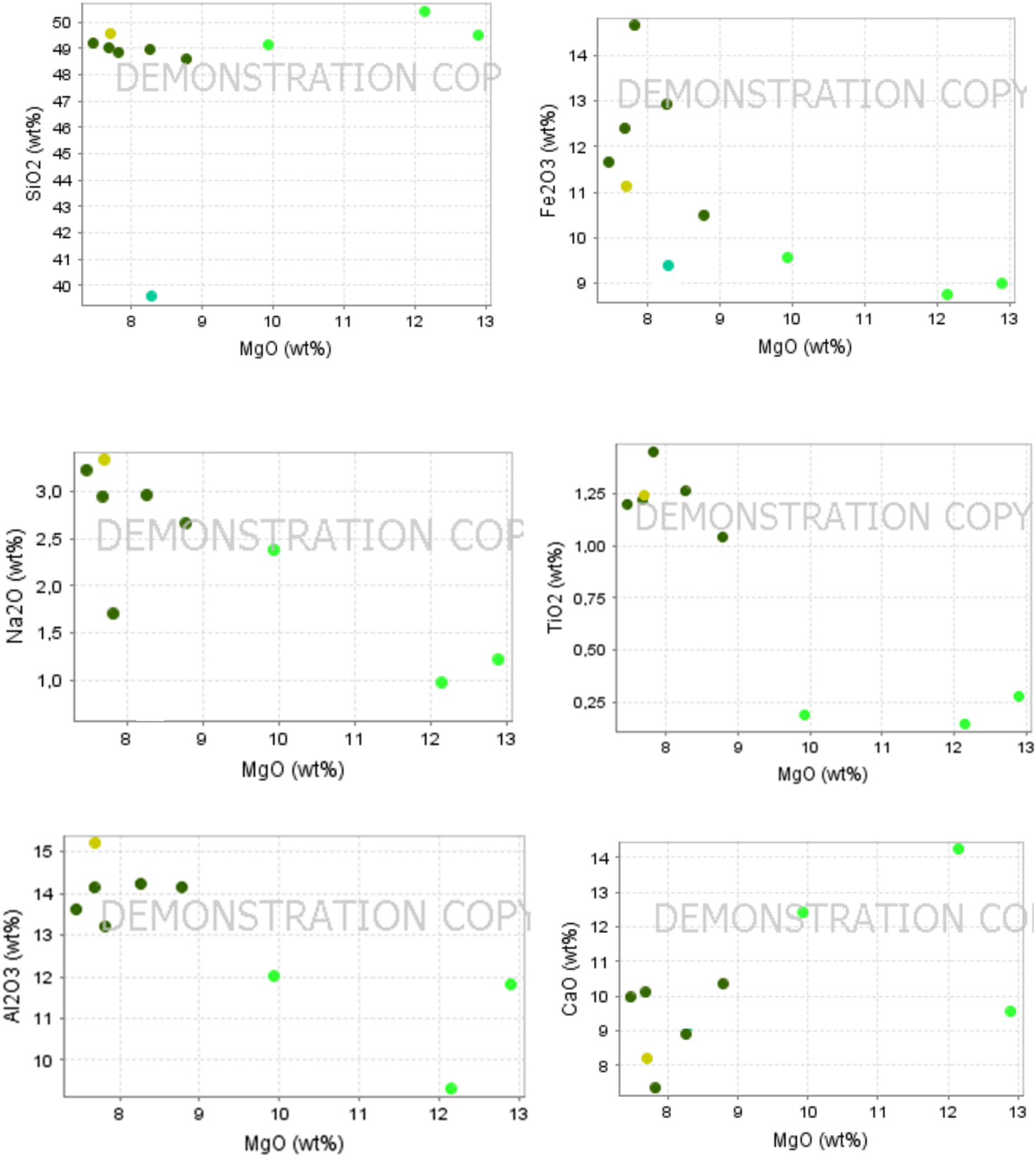

Figure 21. Harker Diagrams for Basalts. Dark green correspond to E-MORB basalts, light green correspond to N-MORB basalts.

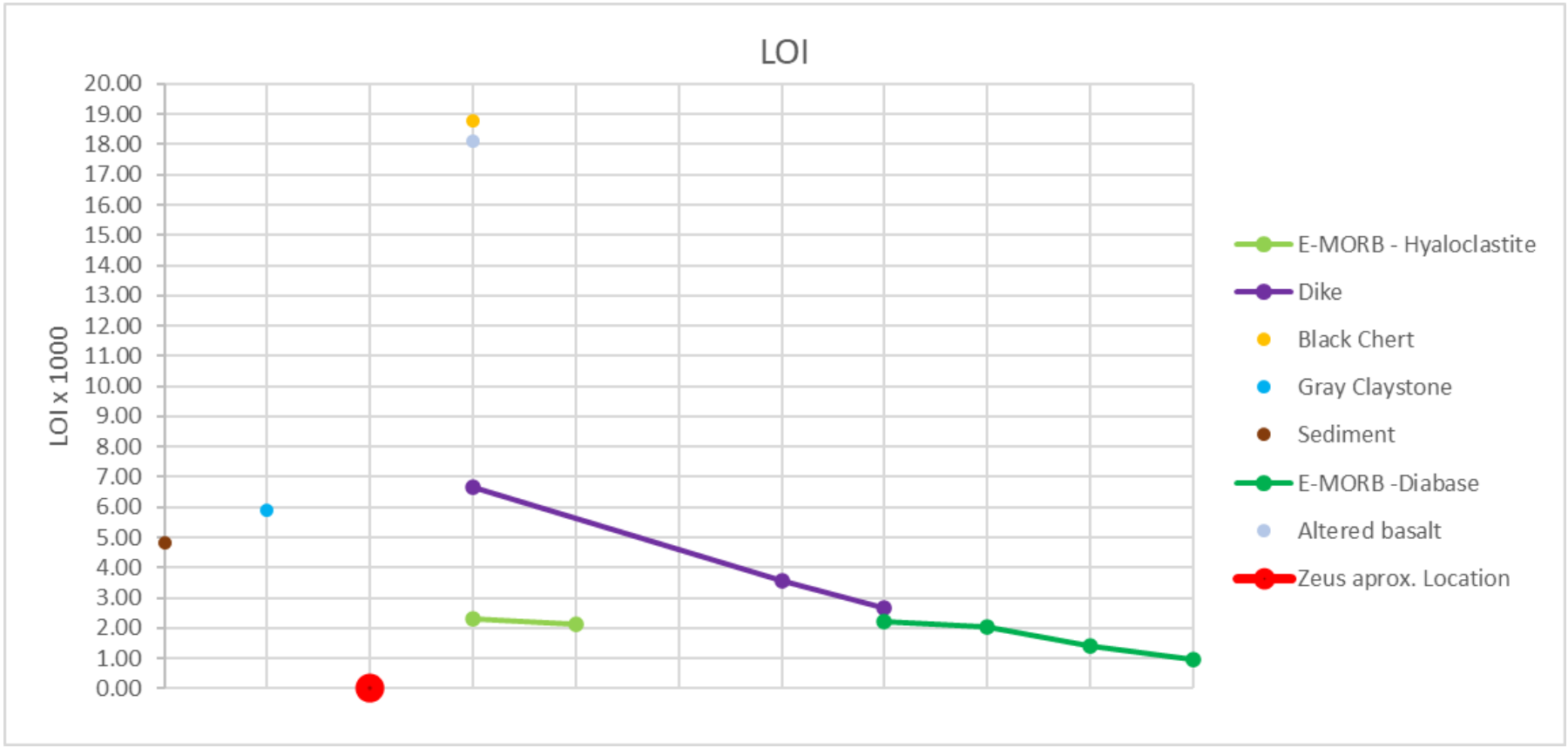

Figure 22. LOI Values for all samples. X-axes correspond to schematic distance to the ore body "Zeus"

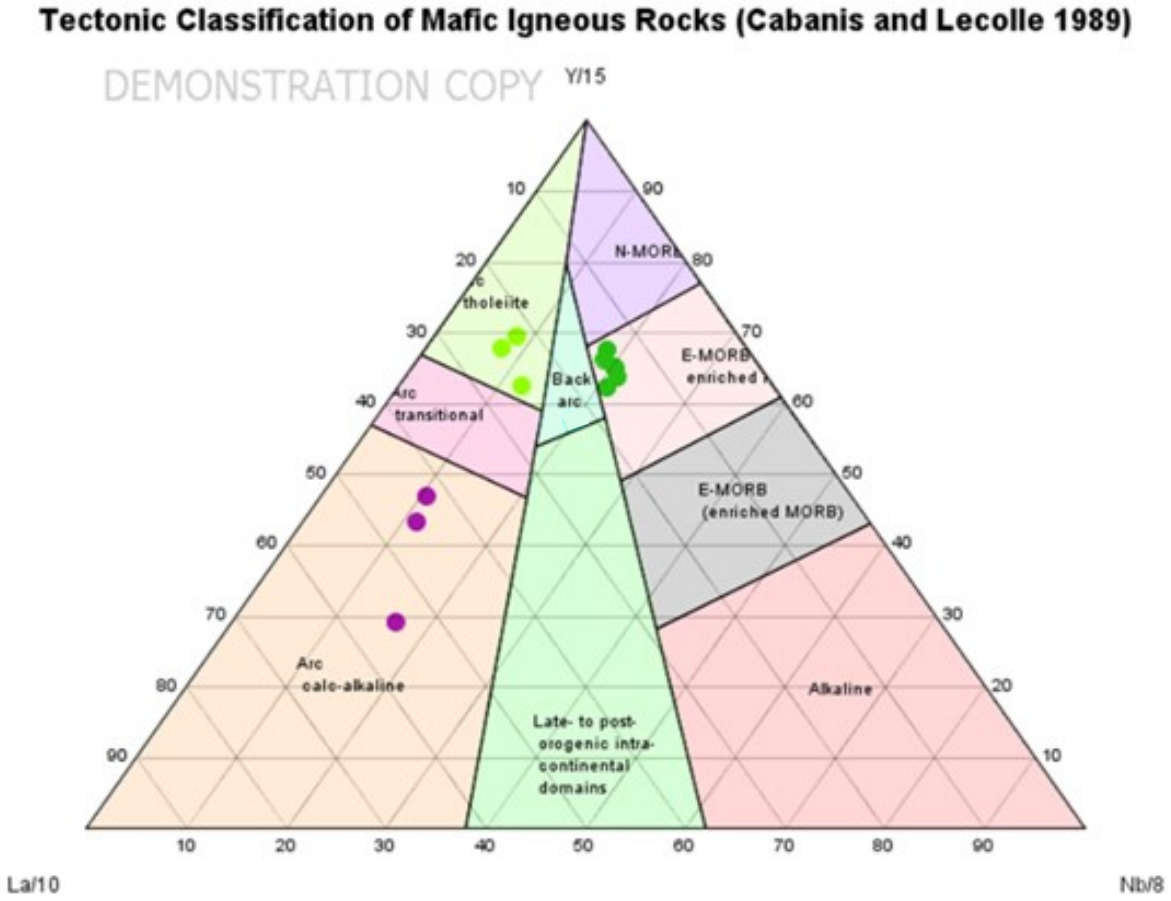

Figure 23. (Cabanis and Lecolle, 1989) Tectonic classification of mafic igneous rocks plotting basalts and dikes. Purple points correspond to dikes, dark green correspond to E-MORB basalts, light green correspond to N-MORB basalts.

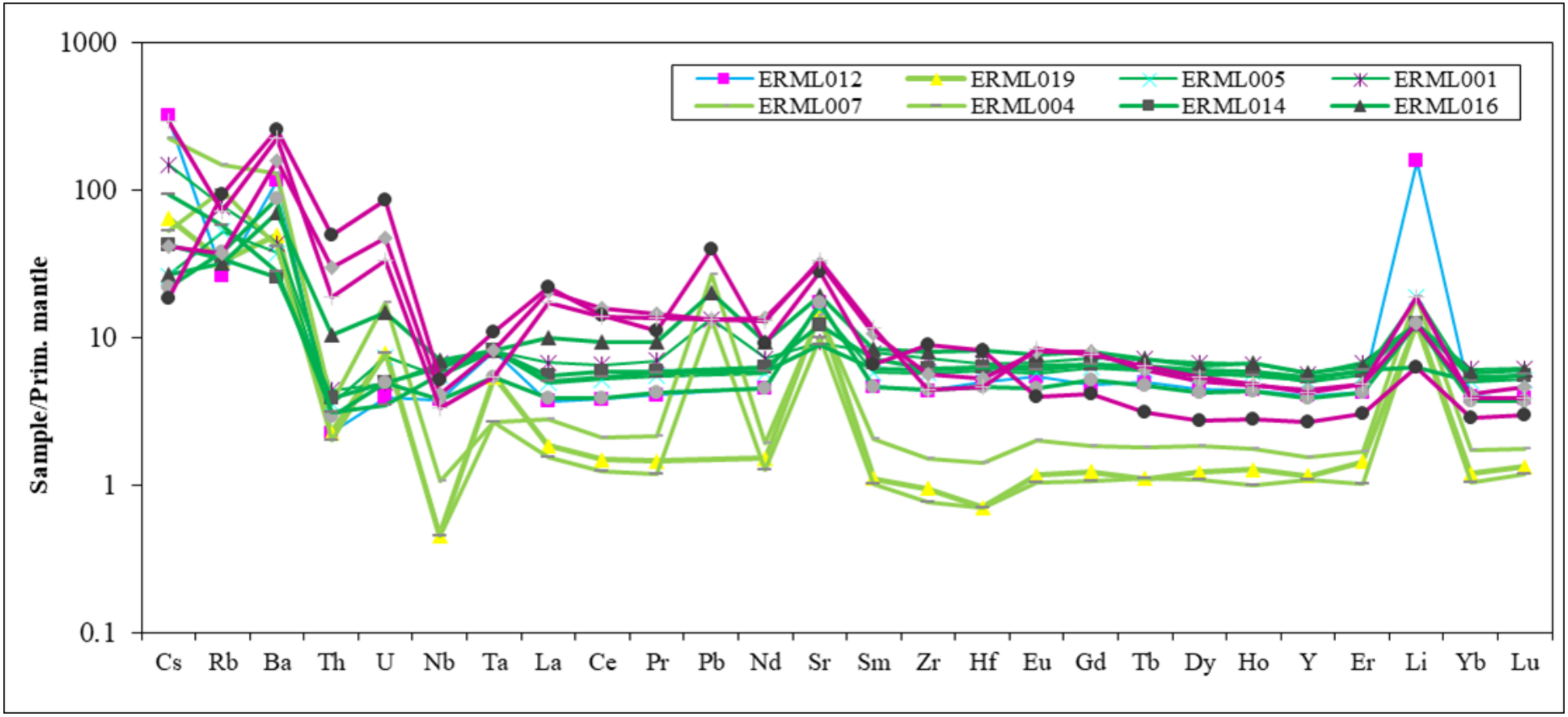

Figure 24. Minor element spider diagram normalized with primitive mantle for basalts (green) and dikes (purple) at El Roble mine (Sun and McDonough, 1989).

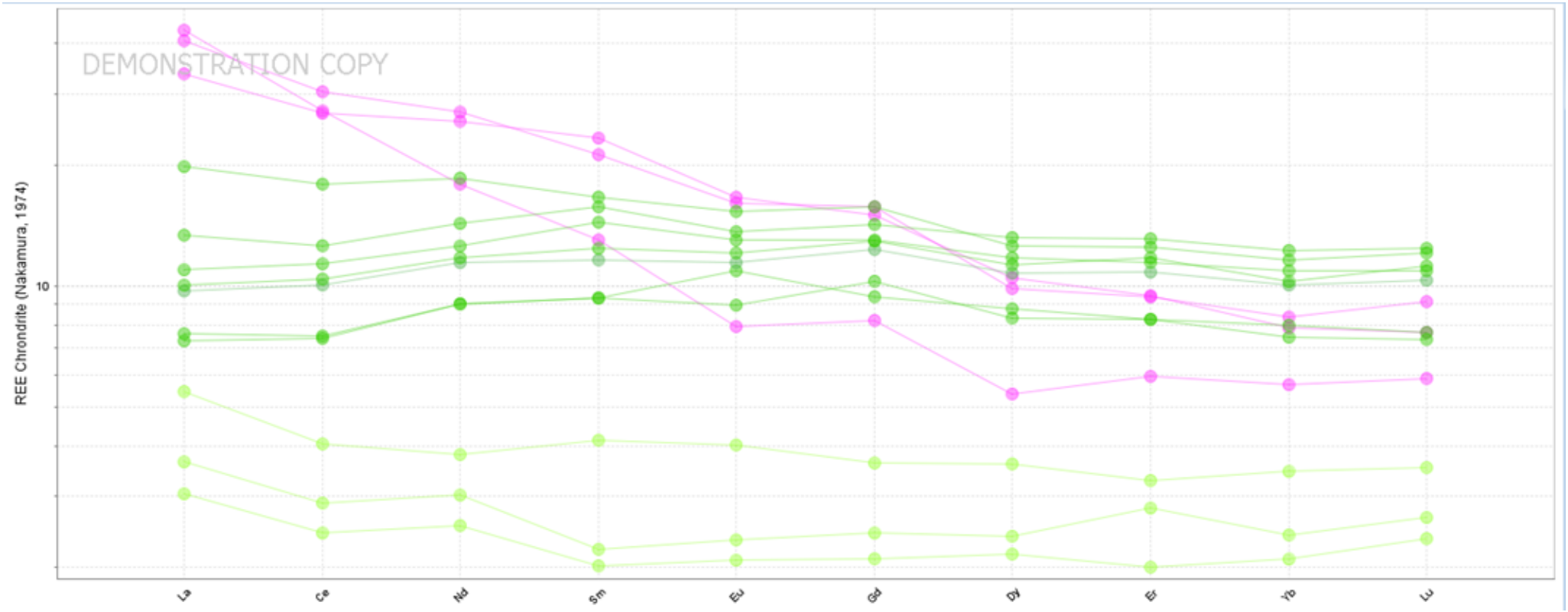

Figure 25. REE normalized with chondrite for basalts (green) and dikes (purple) at El Roble mine (Nakamura, 1974).

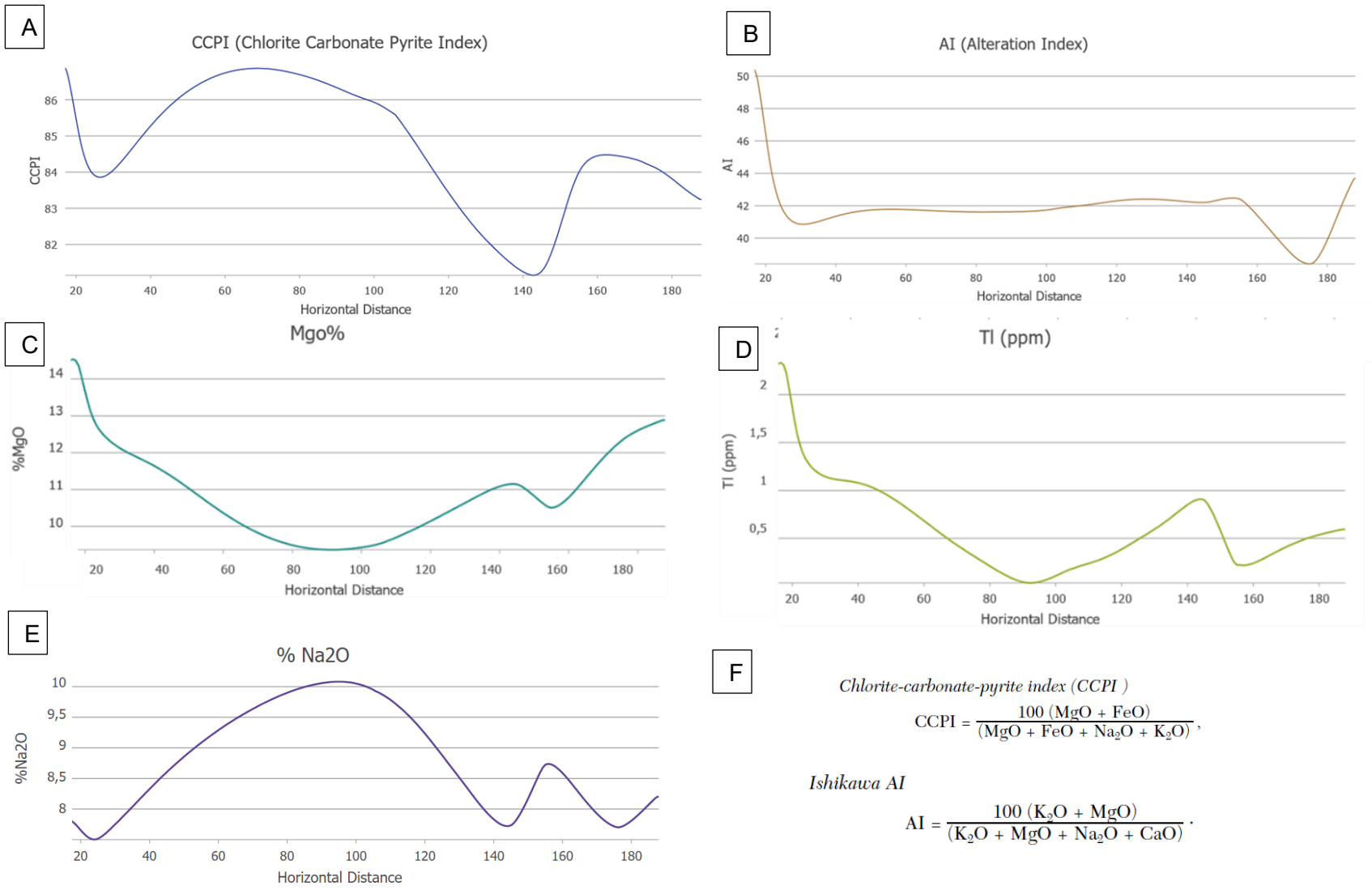

Figure 26. Variations across 1760 transect (A) CCPI (B) AI (C) MgO (D) Tl (E) Na_2O (F) CCPI and AI equations (Large et al., 2001) and (Ishikawa et al., 1976).

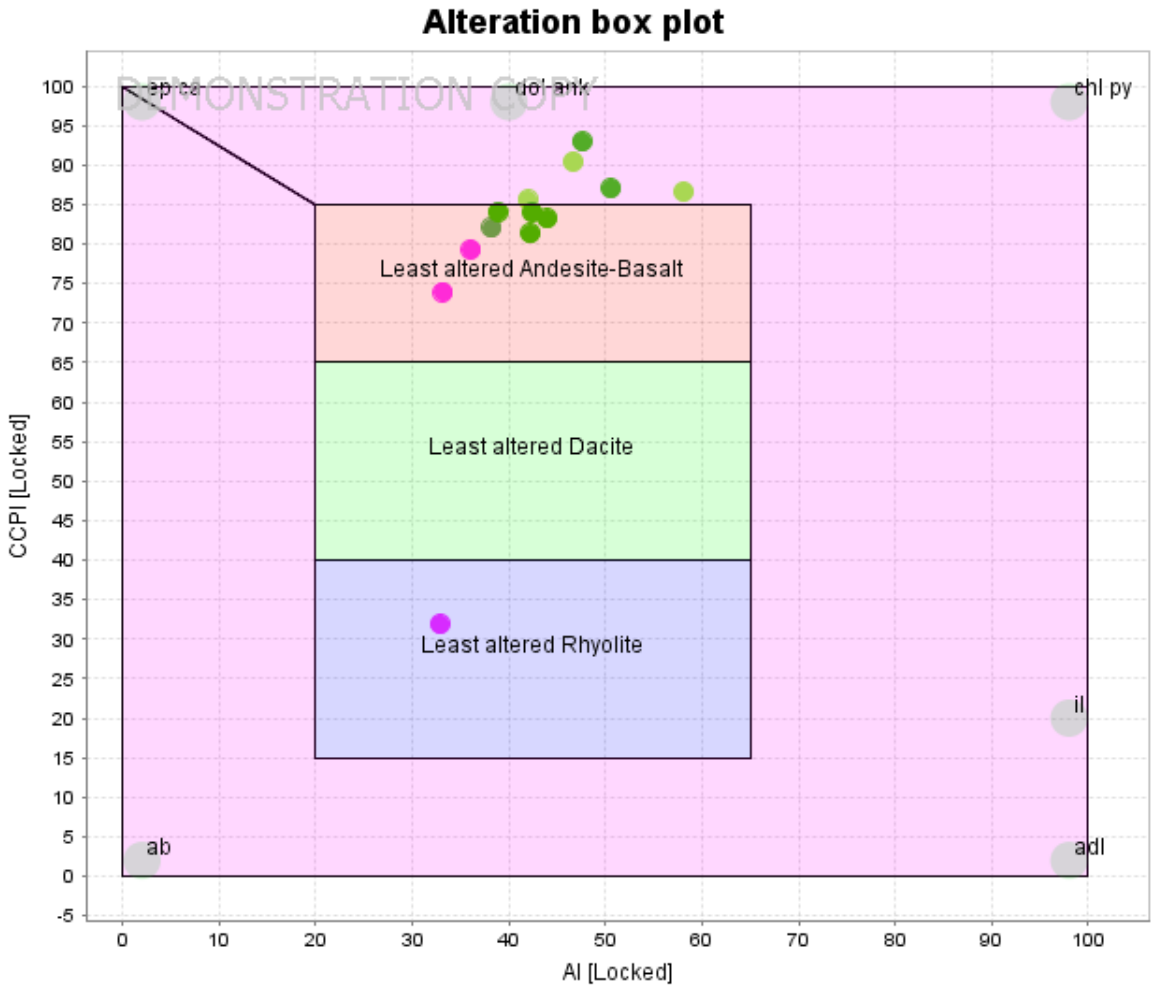

Figure 27. Alteration box plot CCPI vs AI (Large et al., 2001) basalts (green points) dikes (purple points).

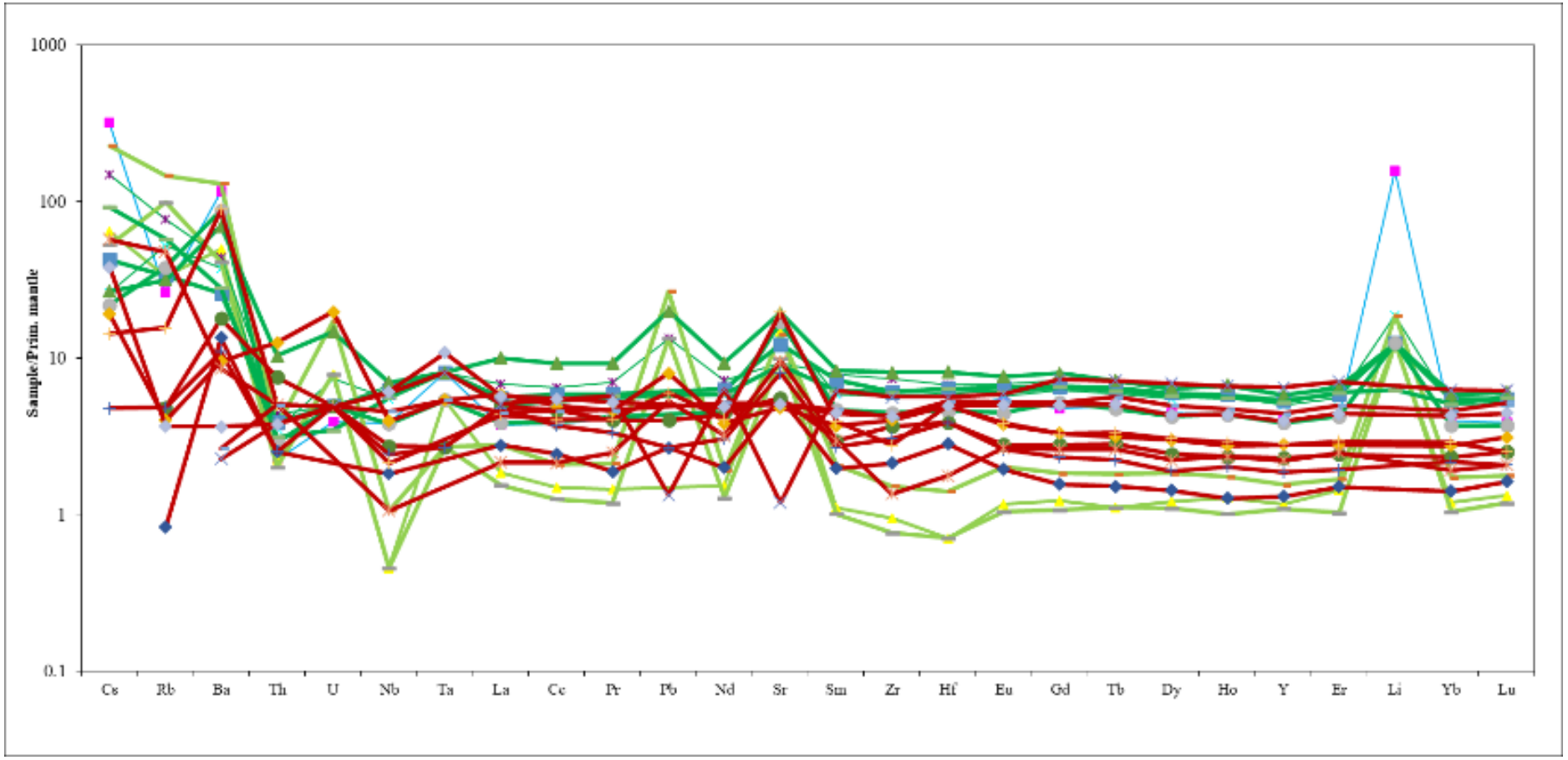

Figure 28. Comparison between El Roble basalts (green and blue lines) and typical Barroso formation at (Rodríguez García and Arango Mejía, 2013) (red lines)

Code	Type	Recvd W	Al2O3	BaO	CaO	Cr2O3	Fe2O3	K2O	MgO	MnO	Na2O	P2O5	SiO2	SrO	TiO2	LOI 100	Total	C	S
		kg	%	%	%	%	%	%	%	%	%	%	%	%	%	%	%	%	%
ERML001	Basalt	0.88	13.21	0.04	7.34	0.01	14.66	1.43	7.82	0.18	1.70	0.12	48.87	0.02	1.45	2.31	104.40	0.10	2.10
ERML002	Claystone	0.81	8.91	1.79	4.72	0.01	3.82	2.04	1.63	0.38	0.54	0.12	69.47	0.04	0.40	5.89	101.30	1.33	0.46
ERML003	Sediment	0.81	8.75	0.37	3.16	0.01	3.48	0.84	1.27	0.16	2.61	0.07	73.12	0.02	0.36	4.82	99.53	1.26	0.16
ERML004	Basalt	0.93	9.30	0.04	14.25	0.23	8.75	1.15	12.15	0.21	0.97	0.03	50.41	0.03	0.15	1.90	99.77	0.22	0.02
ERML005	Basalt	0.96	13.62	0.03	9.96	0.03	11.66	0.70	7.46	0.19	3.23	0.10	49.19	0.04	1.20	2.14	100.65	0.15	0.37
ERML007	Basalt	0.69	11.82	0.10	9.55	0.16	8.98	2.02	12.90	0.14	1.22	0.05	49.52	0.04	0.28	2.08	99.59	0.04	0.23
ERML010	Dique	0.61	14.87	0.17	10.45	<0.01	11.58	2.12	4.83	0.21	1.86	0.45	44.95	0.08	0.94	6.65	100.65	1.60	0.50
ERML011	Black chert	0.53	0.90	0.04	23.50	0.02	0.84	0.24	0.81	0.19	0.01	0.57	53.33	0.03	0.04	18.77	100.45	5.95	0.38
ERML012	Basalt	0.80	12.26	0.08	9.16	0.04	9.38	0.62	8.28	0.15	0.65	0.08	39.58	0.04	0.95	18.10	100.15	4.23	0.27
ERML013	Basalt	0.98	14.23	0.03	8.90	0.03	12.92	1.05	8.26	0.22	2.96	0.10	48.96	0.02	1.26	0.97	101.10	0.05	0.41
ERML014	Basalt	0.78	14.14	0.03	10.10	0.03	12.40	0.61	7.68	0.21	2.95	0.10	49.04	0.03	1.22	1.40	101.85	0.06	0.69
ERML015	Basalt	0.85	14.16	0.07	10.35	0.07	10.50	0.80	8.78	0.21	2.66	0.08	48.59	0.04	1.04	2.21	99.89	0.24	0.07
ERML016	Basalt	0.77	15.22	0.06	8.20	0.02	11.14	0.73	7.70	0.18	3.34	0.20	49.57	0.05	1.24	2.03	101.75	0.12	0.78
ERML017	Dique	0.73	15.09	0.12	8.77	0.01	10.57	1.35	4.85	0.16	3.71	0.38	50.62	0.08	0.88	3.55	105.10	0.63	1.97
ERML018	Dique	0.79	15.48	0.19	5.00	<0.01	2.86	3.49	1.28	0.06	4.75	0.12	62.83	0.07	0.34	2.68	100.10	0.48	0.35
ERML019	Basalt	0.85	12.01	0.05	12.40	0.13	9.55	0.74	9.93	0.22	2.38	0.04	49.13	0.04	0.19	2.37	99.78	0.31	0.19

Table 1. Major elements.

Code	Type	Recvd W	Ba	Ce	Cr	Cs	Dy	Er	Eu	Ga	Gd	Ge	Hf	Ho	La	Lu	Nb	Nd	Pr	Rb	Sm	Sn	Sr	Ta	Tb	Th
		kg	ppm	ppm	ppm	ppm	ppm	ppm	ppm	ppm	ppm	ppi	ppm	ppm	ppm	ppm	ppm	ppm	ppm	ppm	ppm	ppm	ppm	ppm	ppm	ppm
ERML001	Basalt	0.88	287.00	10.90	100.00	3.11	4.53	2.95	1.05	18.10	3.93	<5	1.90	0.99	4.40	0.42	4.40	9.00	1.78	46.30	3.19	1.00	185.00	0.30	0.71	0.35
ERML002	Claystone	0.81	>10000	36.40	50.00	4.80	4.80	2.70	0.91	16.40	5.01	<5	2.60	0.94	26.10	0.39	7.30	24.90	6.03	67.30	5.37	1.00	300.00	0.60	0.78	6.53
ERML003	Sediment	0.81	3820.00	16.40	50.00	1.53	1.90	1.36	0.50	10.60	2.05	<5	2.30	0.43	9.00	0.19	3.50	8.80	2.24	23.00	2.06	1.00	169.50	0.30	0.34	3.51
ERML004	Basalt	0.93	271.00	2.10	1600.00	1.11	0.74	0.45	0.16	8.60	0.58	<5	0.20	0.15	1.00	0.08	0.30	1.60	0.30	59.50	0.41	<1	198.00	0.10	0.11	0.16
ERML005	Basalt	0.96	247.00	8.70	200.00	0.55	3.69	2.43	0.88	15.60	3.40	<5	1.70	0.85	3.20	0.35	3.60	7.20	1.39	31.40	2.36	1.00	317.00	0.30	0.59	0.28
ERML007	Basalt	0.69	864.00	3.50	1180.00	4.76	1.24	0.74	0.31	9.60	1.00	<5	0.40	0.26	1.80	0.12	0.70	2.40	0.54	87.90	0.84	<1	282.00	0.10	0.18	0.29
ERML010	Dique	0.61	1480.00	23.20	30.00	6.17	3.60	2.13	1.28	16.30	4.15	<5	1.30	0.72	11.10	0.26	2.20	16.20	3.44	43.50	4.73	1.00	669.00	0.20	0.63	1.49
ERML011	Black chert	0.53	273.00	3.30	110.00	0.65	1.21	0.98	0.17	5.60	1.10	<5	0.20	0.31	9.30	0.12	0.60	4.30	0.96	5.90	0.81	<1	219.00	0.10	0.17	0.33
ERML012	Basalt	0.80	769.00	6.40	260.00	6.67	3.01	1.86	0.84	13.00	2.60	<5	1.40	0.66	2.40	0.26	2.50	5.70	1.04	15.80	1.89	<1	343.00	0.30	0.49	0.18
ERML013	Basalt	0.98	186.00	9.00	230.00	1.94	3.88	2.64	0.93	16.10	3.56	<5	1.80	0.83	3.30	0.38	3.70	7.40	1.46	34.60	2.51	1.00	179.00	0.30	0.61	0.25
ERML014	Basalt	0.78	170.50	9.80	230.00	0.89	4.04	2.58	1.00	16.50	3.58	<5	1.80	0.87	3.60	0.37	4.10	7.90	1.50	20.20	2.92	1.00	244.00	0.30	0.64	0.31
ERML015	Basalt	0.85	582.00	6.50	440.00	0.46	2.86	1.86	0.69	15.00	2.84	<5	1.30	0.65	2.50	0.25	2.50	5.70	1.07	22.90	1.90	1.00	341.00	0.20	0.47	0.23
ERML016	Basalt	0.77	461.00	15.50	160.00	0.56	4.31	2.81	1.18	17.10	4.34	<5	2.30	1.00	6.50	0.41	4.60	11.70	2.36	19.00	3.38	1.00	387.00	0.30	0.71	0.82
ERML017	Dique	0.73	1035.00	26.30	60.00	0.87	3.38	2.11	1.24	16.60	4.34	<5	1.50	0.71	13.40	0.31	2.70	17.00	3.66	22.50	4.30	1.00	633.00	0.30	0.59	2.36
ERML018	Dique	0.79	1695.00	23.50	20.00	0.39	1.85	1.34	0.61	14.10	2.27	<5	2.30	0.42	14.20	0.20	3.40	11.30	2.82	56.30	2.64	1.00	552.00	0.40	0.31	3.96
ERML019	Basalt	0.85	328.00	2.50	950.00	1.35	0.82	0.63	0.18	8.50	0.67	<5	0.20	0.19	1.20	0.09	0.30	1.90	0.37	19.90	0.45	<1	294.00	0.20	0.11	0.18

Table 2. Minor and REE elements.

Tm	U	V	W	Y	Yb	Zr	As	Bi	Hg	In	Re	Sb	Sc	Se	Te	Tl	Ag	Cd	Co	Cu	Li	Mo	Ni	Pb	Sc	Zn
ppm	ppm	ppm	ppm	ppm	ppm	ppm	ppm	ppm	ppm	ppm	ppm	ppm	ppm	ppm	ppm	ppm	ppm	ppm	ppm	ppm	ppm	ppm	ppm	ppm	ppm	ppm
0.43	0.10	407.00	2.00	24.50	2.70	77.00	0.60	0.13	<0.005	0.02	0.01	0.09	10.80	2.40	0.09	0.49	<0.5	1.00	51.00	133.00	20.00	<1	73.00	2.00	43.00	201.00
0.39	2.45	86.00	3.00	26.50	2.43	98.00	2.70	0.22	0.17	0.04	<0.001	0.59	4.20	0.50	0.05	0.14	<0.5	<0.5	11.00	1350.00	20.00	1.00	61.00	21.00	12.00	138.00
0.22	1.05	71.00	3.00	11.70	1.30	90.00	2.50	0.12	0.26	0.02	<0.001	0.24	3.80	0.40	0.02	0.04	<0.5	<0.5	8.00	42.00	90.00	1.00	28.00	4.00	9.00	66.00
0.08	0.16	150.00	1.00	4.70	0.46	8.00	1.40	0.04	0.04	<0.005	0.02	0.06	1.70	0.20	0.10	0.17	<0.5	0.60	52.00	4.00	20.00	18.00	443.00	2.00	29.00	132.00
0.37	0.15	348.00	2.00	21.50	2.21	60.00	1.00	0.06	0.02	0.02	0.00	0.10	6.70	0.80	0.15	0.05	<0.5	0.80	44.00	99.00	30.00	<1	98.00	<2	44.00	130.00
0.12	0.35	179.00	1.00	6.70	0.76	16.00	0.60	0.06	0.08	0.01	0.00	0.08	5.50	0.90	0.29	0.70	<0.5	0.60	47.00	85.00	30.00	1.00	318.00	4.00	33.00	117.00
0.29	0.68	343.00	1.00	18.40	1.73	47.00	3.40	0.03	0.31	0.06	<0.001	0.37	27.50	0.80	0.02	0.86	<0.5	0.80	31.00	166.00	30.00	<1	21.00	2.00	33.00	115.00
0.15	2.95	212.00	1.00	14.70	0.88	10.00	13.40	0.04	1.86	0.01	0.02	3.59	1.30	13.60	0.19	0.15	2.80	12.60	2.00	74.00	<10	6.00	63.00	3.00	2.00	511.00
0.25	0.08	251.00	4.00	17.30	1.76	46.00	16.10	0.01	0.62	0.05	0.00	2.53	32.80	0.60	0.02	0.09	<0.5	0.70	36.00	104.00	250.00	<1	84.00	<2	36.00	72.00
0.36	0.07	338.00	1.00	22.40	2.25	63.00	0.40	0.04	0.01	0.02	0.00	<0.05	7.70	0.60	0.07	0.29	<0.5	1.10	48.00	118.00	10.00	<1	108.00	<2	47.00	101.00
0.39	0.10	362.00	1.00	23.00	2.40	64.00	0.60	0.08	0.05	0.01	0.00	0.08	4.70	0.50	0.08	0.08	<0.5	0.70	45.00	157.00	20.00	2.00	98.00	<2	46.00	105.00
0.27	0.10	261.00	1.00	16.60	1.64	47.00	1.40	0.04	0.07	0.01	0.00	0.21	6.20	0.20	0.07	0.04	<0.5	0.70	43.00	41.00	20.00	1.00	150.00	<2	40.00	138.00
0.39	0.30	281.00	1.00	24.90	2.55	85.00	0.40	0.06	0.07	0.01	0.00	0.10	6.30	0.90	0.11	0.04	<0.5	0.90	40.00	120.00	20.00	<1	70.00	3.00	36.00	88.00
0.30	0.97	299.00	2.00	19.20	1.84	59.00	0.40	0.17	0.09	0.03	0.00	0.05	12.20	2.20	0.42	0.03	<0.5	0.80	27.00	254.00	20.00	1.00	27.00	2.00	32.00	64.00
0.19	1.73	73.00	1.00	11.40	1.25	93.00	0.20	0.03	0.03	0.01	<0.001	0.19	2.80	0.70	0.07	0.02	<0.5	<0.5	7.00	48.00	10.00	1.00	10.00	6.00	6.00	39.00
0.08	0.16	168.00	2.00	5.00	0.53	10.00	1.70	0.02	0.03	0.01	0.00	0.40	4.90	0.20	0.09	0.07	<0.5	0.80	50.00	31.00	20.00	1.00	245.00	<2	32.00	105.00

Table 3. Continuation of minor and REE elements.